lack of relevant data, such as a pK_a for HIO_2. The mechanism confirms, for the first time, a significant role for IBr in mixed oxyhalogen kinetics and augments the number of complex networks incorporating bromine(III) reactions for which a mechanistic explanation is available.

Acknowledgment. We thank Dr. István Lengyel for many helpful discussions and for the use of his kinetic modeling program. This work was supported by Research Grant CHE-9023294 from the National Science Foundation and by Conselho Nacional de Desenvolvimento Científico e Technológico-CNPq (proc. 202081/90-7).

Registry No. BrO_2^-, 15477-77-7; I^-, 20461-54-5.

Electronic Spectroscopy of Jet-Cooled Half-Sandwich Organometallic Complexes CaC_5H_5, $CaC_5H_4CH_3$, and CaC_4H_4N

Eric S. J. Robles,[†] Andrew M. Ellis,[‡] and Terry A. Miller*

Contribution from the Laser Spectroscopy Facility, Department of Chemistry, The Ohio State University, 120 West 18th Avenue, Columbus, Ohio 43210. *Received March 10, 1992*

Abstract: Laser excitation and dispersed fluorescence spectra of jet-cooled, open-faced organometallic complexes, CaC_5H_5, $CaC_5H_4CH_3$, and CaC_4H_4N, are presented and analyzed. The electronic structure of these molecules can best be described as Ca^+ being perturbed by R^- (R = C_5H_5, $C_5H_4CH_3$, and C_4H_4N). The electronic transitions observed here are essentially metal-centered. The electronic spectra of these complexes show extensive vibrational structure arising from excitation of skeletal and intra-ring modes. From this structure, we are able to determine the binding site of the metal atom, i.e., above the ring in a pentahapto (η^5) bonding fashion. The electronic spectra of the fully-deuterated isotopomers CaC_5D_5 and CaC_4D_4N are also presented here to provide information about "pure" hydrogenic vibrations in CaC_5H_5 and CaC_4H_4N. Several vibronic bands of CaC_5H_5 are also attributed to single quantum excitation of e_2 modes, which indicates that this molecule is Jahn–Teller active in its $\tilde{A}^2E_1$ electronic state. In the case of $CaC_5H_4CH_3$, methyl torsional bands are observed, from which the barrier to methyl free rotation and the change in conformation of the methyl group on $\tilde{A}$–$\tilde{X}$ excitation are determined. This study represents the first spectroscopic study on $CaC_5H_4CH_3$ in the gas phase.

I. Introduction

The full-sandwich compound bis(cyclopentadienyl)calcium or calcocene, $Ca(C_5H_5)_2$ (or $CaCp_2$ for short), was synthesized first by Cotton and Wilkinson in 1954.[1] Since then $CaCp_2$ and its ring-substituted derivatives have been structurally and spectroscopically characterized.[2-7] A single X-ray crystallographic diffraction study showed that $CaCp_2$ (ref 4) has a polymeric structure in the solid state, in which four Cp rings are coordinated to each calcium atom in an η^1, η^3, η^5, η^5 fashion (the η^n notation means that there are n ligand atoms bonded to the metal). Unfortunately, because of the polymeric nature of solid $CaCp_2$, its volatility is extremely low, which prevented a molecular structure determination of this compound in the gas phase.[5] The only available gas-phase work on $CaCp_2$ is a mass spectrometric study of this molecule, which showed that the most abundant molecular ions are $CaCp_2^+$ and $CaCp^+$.[4] The low-volatility problem in polymeric $CaCp_2$ was later resolved by completely substituting a methyl group for each of the five hydrogens in the Cp ring, to give the monomeric pentamethylcyclopentadienyl complex $Ca(C_5Me_5)_2$. A gas-phase electron diffraction study of $Ca(C_5Me_5)_2$ revealed that the two C_5Me_5 ligands are both η^5-bonded but are nonparallel, i.e., η^5-$Ca(C_5Me_5)_2$ is bent.[7] Ab initio calculations on $CaCp_2$ were performed but failed to explain why $Ca(C_5Me_5)_2$ has a bent structure and not the regular sandwich structure with parallel Cp rings.

Recently, Bernath and co-workers[8,9] reported laser spectroscopic studies on the half-sandwich complexes CaCp and CaC_4H_4N (CaPy). Unlike the closed-shell species $CaCp_2$, CaCp and CaPy are chemically unstable transient species, so-called organometallic free radicals. Bernath and co-workers prepared these molecules in the gas phase using the Broida oven technique, in which the metal (Ca) was evaporated from a resistively heated alumina crucible, after which the metal vapor is mixed with an appropriate oxidant gas under flowing conditions yielding the desired molecular species. In addition to CaCp and CaPy, a number of radicals of the type M–R, where M is an alkaline earth metal (Ca, Sr, Ba) and R is an organic ligand (e.g., methyl (CH_3),[10,11] methoxy (OCH_3),[12,13] Cp,[8] and Py[9]), have been studied.

A drawback of the Broida oven method is that molecules are produced with relatively high internal temperatures, 500 K being a typical rotational temperature. This results in substantial spectral congestion. For example, in a laser-induced fluorescence (LIF) study of CaCp[8] and CaC_4H_4N (CaPy),[9] the relatively high temperatures resulted in bands with full width at half-maximum (fwhm) of the order of 50 cm^{-1}. With this resolution, closely

* Corresponding author.
† 1991 Rohm and Haas and 1992 Phillips Petroleum Fellow.
‡ NATO/SERC and Ohio State Postdoctoral Fellow. Present address: Department of Chemistry, University of Leicester, University Road, Leicester LE1 7RH, England.

(1) Wilkinson, G.; Cotton, F. A. *Chem. Ind. (London)* **1954**, *11*, 307.
(2) Fischer, E. O.; Stolzle, G. *Chem. Ber.* **1961**, *94*, 2187.
(3) Allan, K. A.; Gowenlock, B. G.; Lindsell, W. E. *J. Organomet. Chem.* **1973**, *55*, 229.
(4) Zerger, R.; Stucky, G. *J. Organomet. Chem.* **1974**, *80*, 7.
(5) Blom, R.; Faegri, K., Jr.; Volden, H. V. *Organometallics* **1990**, *9*, 372.
(6) Gardiner, M. G.; Raston, C. L.; Kennard, C. H. L. *Organometallics* **1991**, *10*, 3680.
(7) Andersen, R. A.; Boncella, J. M.; Burns, C. J.; Blom, R.; Haaland, A.; Volden, H. V. *J. Organomet. Chem.* **1986**, *312*, C49.
(8) O'Brien, L. C.; Bernath, P. F. *J. Am. Chem. Soc.* **1986**, *108*, 5017.
(9) Bopegedera, A. M. R. P.; Fernando, W. T. M. L.; Bernath, P. F. *J. Phys. Chem.* **1990**, *94*, 4476.
(10) Brazier, C. R.; Bernath, P. F. *J. Chem. Phys.* **1987**, *86*, 5918.
(11) Brazier, C. R.; Bernath, P. F. *J. Chem. Phys.* **1989**, *91*, 4548.
(12) Brazier, C. R.; Ellingboe, L. C.; Kinsey-Nielson, S.; Bernath, P. F. *J. Am. Chem. Soc.* **1986**, *108*, 2126.
(13) O'Brien, L. C.; Brazier, C. R.; Bernath, P. F. *J. Mol. Spectrosc.* **1988**, *130*, 33.

0002-7863/92/1514-7171$03.00/0

spaced vibrational structure cannot be resolved and there is therefore less information extracted from the spectra than is potentially available if the structure were resolved.

With the recent development of a pulsed-laser vaporization/photolysis method for preparing organometallic radicals in our laboratory,[14] we can now produce these species in the ultracold environment of a supersonic jet expansion. In this method, a metal rod and an organic precursor are simultaneously vaporized and photolyzed, respectively, by an excimer laser beam. By employing this technique, we have obtained electronic spectra of a number of previously unobserved organometallic radicals, namely, those in which the metal is zinc, cadmium, or magnesium. The list includes ZnCp, ZnPy, ZnMeCp, and the corresponding cadmium- and magnesium-containing species (MeCp = methylcyclopentadienyl ($C_5H_4CH_3$)).[14-18]

In this paper, we employ our pulsed-laser vaporization/photolysis technique to investigate the electronic spectra of CaCp and CaPy. From our spectra, the rotational temperature of these molecules is $\lesssim$5 K corresponding to vibronic bands having fwhm of $\sim$2.5 cm^{-1}. This allows us to observe much more extensive vibrational structure than possible in previous studies of these molecules by Bernath et al.[8,9] Here, we will present our vibrational analysis of this structure. To assist the analysis, particularly for those modes involving hydrogenic motion, we also present the excitation spectra of the fully-deuterated derivatives of CaCp and CaPy, which we will refer to as d_5-CaCp and d_4-CaPy, respectively. We also include a study on another half-sandwich complex of Ca which has not been observed before, that where the organic ligand is methylcyclopentadienyl (MeCp). In CaCp, the metal is ring-bonded giving this molecule C_{5v} symmetry. In CaMeCp, we expect its molecular structure to be similar to CaCp, i.e., the metal atom is also ring-bonded. However, the presence of the methyl group reduces the point group symmetry to C_s (assuming the methyl group is a structureless ball), thereby lifting any electronic and vibrational degeneracies initially present under C_{5v} symmetry. Despite the symmetry lowering in passing from C_{5v} to C_s point group, one would still expect the vibrational structure in their spectra to have notable similarities. By employing such an analogy, we have assigned the vibrational structure in the laser excitation and dispersed fluorescence spectra of CaMeCp and this will also be discussed here.

Furthermore, very low-frequency, irregularly spaced bands are observed in both excitation and dispersed fluorescence spectra of CaMeCp. This structure is attributed to hindered rotation of the methyl group, from which the barrier to methyl free rotation in both the ground ($\tilde{X}$) and excited ($\tilde{A}$) electronic states and the change in conformation of the methyl group upon electronic excitation have been determined. This report should be an important addition to the current information on hindered methyl rotation phenomena in open-shell species, which at present is limited to a small number of radicals such as *o*-, *m*-, and *p*-methyl benzyls,[19] MeCp,[20] the inert gas–radical complex MeCp–He_2,[21] and the organometallic radicals ZnMeCp and CdMeCp.[18]

II. Experimental Section

The pulsed-laser vaporization/photolysis technique employed in these experiments to prepare the (i) CaCp, (ii) CaMeCp, and (iii) CaPy radicals in the gas phase has been described previously.[14,15] Briefly, the organic precursors used are (i) liquid cyclopentadiene monomer (C_5H_6, obtained by cracking (distilling) cyclopentadiene dimer $(C_5H_6)_2$, 99%, Aldrich), (ii) liquid methylcyclopentadiene monomer ($C_5H_5CH_3$, obtained by cracking methylcyclopentadiene dimer $(C_5H_5CH_3)_2$, 95% Aldrich), and (iii) liquid pyrrole (C_4H_4NH, 99%, Aldrich). These precursors were placed in a stainless steel bomb immersed in a constant temperature bath. We found that the temperature of the bath is extremely critical in obtaining cold spectra of these molecules. For both C_5H_6 and $C_5H_5CH_3$, an acetone–dry ice (−78 °C) bath was used while for C_4H_4NH (mp = −23 °C), a refrigerated circulating bath was maintained at a bath temperature of −15 °C.

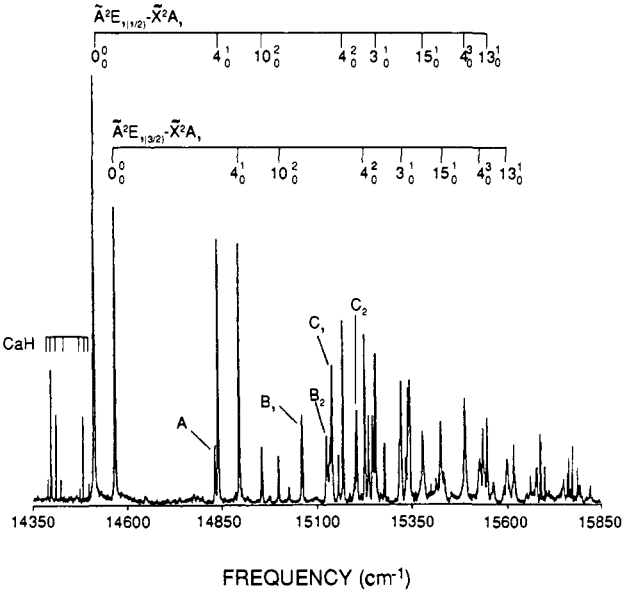

Figure 1. Laser excitation spectrum of CaCp covering the $\tilde{A}^2E_1$–$\tilde{X}^2A_1$ band system. The 56-cm^{-1} doubling of bands is attributed to spin–orbit splitting in the $\tilde{A}^2E_1$ state. In addition to CaCp bands, the two spin–orbit components of the $A^2\Pi$–$X^2\Sigma^+$ 0–0 band of CaH are observed, separated by $\sim$80 cm^{-1}.

Deuteration of C_5H_6 was achieved by a base-catalyzed H–D exchange reaction.[22] Briefly, 20 mL of C_5H_6, 55 mL of D_2O (99.9 atom % D), and 0.6 mL of 30 wt % NaOD in D_2O (99+ atom % D) were added to 210 mL of hexamethylphosphoric triamide (HMP). All these chemicals were purchased from Aldrich and were used without further purification. The exchange reaction was allowed to occur at room temperature for 1.5 h with nonstop stirring. The deuterated cyclopentadiene was then distilled at $\sim$42 °C. Mass spectroscopic identification of the products showed that two successive exchanges yield a product of 2:1 ratio of C_5D_6/C_5D_5H.

On the other hand, deuteration of pyrrole was achieved using an acid-catalyzed H–D exchange reaction.[23] Here, 100 mL of 0.1 N D_2SO_4 was prepared by mixing 100 mL of D_2O and 0.5 mL of concentrated H_2SO_4. 20 mL of pyrrole was mixed with 25 mL of 0.1 N D_2SO_4, and the mixture was continuously stirred for 1 h. The acid layer was then removed and substituted by fresh 25 mL of 0.1 N D_2SO_4. This procedure was repeated four times. The final product was then distilled (bp = 131 °C). Mass spectroscopic analysis of the distillate showed a 5:2 mixture of d_4- and d_5-pyrrole.

To prepare the CaCp, CaMeCp, and CaPy radicals, the organic precursor vapor was seeded into a carrier gas by passing helium over the liquid precursor at a pressure of $\sim$250 psig. An excimer laser operating with KrF (248 nm) or ArF (193 nm) fills was employed to simultaneously photolyze the appropriate organic precursor and vaporize the Ca metal sample, after which the reaction products were cooled in a supersonic expansion and probed using LIF spectroscopy.

Laser excitation spectra were taken by scanning a nitrogen-laser-pumped dye laser (Molectron DL-II pumped by a Molectron UV-24) and monitoring the total fluorescence with a photomultiplier tube. The signal was then amplified and transferred to a PC XT computer (via a home-built interface), where it was averaged for a certain number of laser shots and then stored for subsequent analysis. All excitation spectra are shown here with no corrections for variations in dye laser intensity as a function of wavelength.

(14) Ellis, A. M.; Robles, E. S. J.; Miller, T. A. *J. Chem. Phys.* **1991**, *94*, 1752.
(15) Robles, E. S. J.; Ellis, A. M.; Miller, T. A. *J. Phys. Chem.* **1992**, *96*, 3247.
(16) Robles, E. S. J.; Ellis, A. M.; Miller, T. A. *J. Phys. Chem.*, submitted for publication.
(17) Robles, E. S. J.; Ellis, A. M.; Miller, T. A. *J. Phys. Chem.* **1992**, *96*, 3258.
(18) Robles, E. S. J.; Ellis, A. M.; Miller, T. A. *J. Chem. Soc., Faraday Trans.*, in press.
(19) Lin, T.-Y. D.; Miller, T. A. *J. Phys. Chem.* **1990**, *94*, 3554.
(20) Yu, L.; Cullin, D. W.; Williamson, J. M.; Miller, T. A. *J. Chem. Phys.* **1991**, *95*, 804.
(21) Yu, L.; Williamson, J. M.; Foster, S.; Miller, T. A., to be submitted for publication.
(22) Gallinella, E.; Mirone, P. *J. Labelled Compd.* **1971**, *7*, 183.
(23) Bak, B.; Christensen, D.; Hansen, L.; Rastrup-Andersen, J. *J. Chem. Phys.* **1956**, *24*, 720.

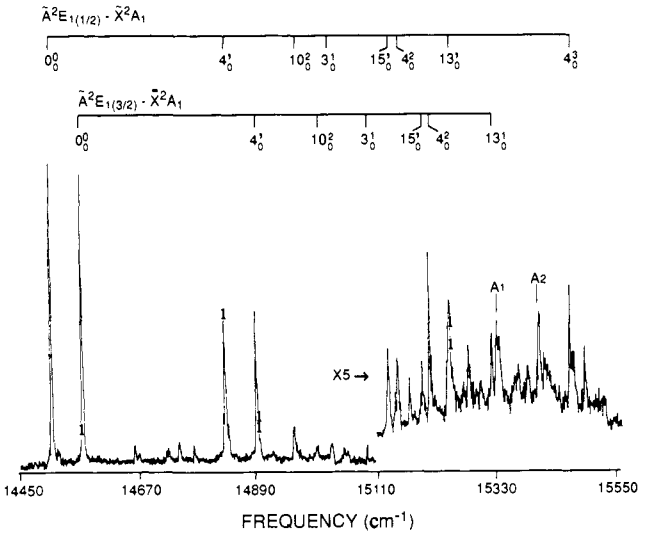

Figure 2. Laser excitation spectrum of d_5-CaCp. The spin–orbit splitting in the $\tilde{A}$ state is found to be the same as in CaCp (56 cm^{-1}).

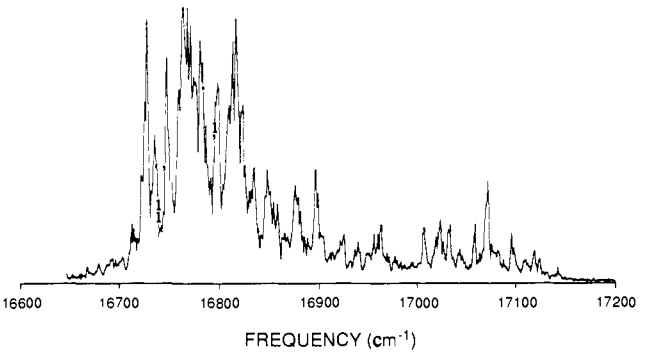

Figure 3. Laser excitation spectrum of CaCp, which was attributed to the "$\tilde{B}^2A_1$–$\tilde{X}^2A_1$" band system by O'Brien and Bernath.[8] See text for more details.

For dispersed fluorescence experiments, where higher attainable dye laser pulse energies were necessary to obtain a good signal-to-noise ratio, we used an excimer-laser-pumped dye laser (Lumonics HD-300 pumped by a Questek Series 2000 excimer laser) to pump a known vibronic transition. The fluorescence was dispersed by a 0.3-m monochromator and then detected by a 1024-element silicon photodiode array detector. The output from the detector was then processed and stored by an optical multichannel analyzer for subsequent analysis. The resulting dispersed fluorescence spectrum was calibrated using an Fe/Ne hollow cathode lamp. The detector was run in gated mode to eliminate, as much as possible, any contributions from scattered dye laser light.

III. Results and Discussion

Laser excitation and dispersed fluorescence spectra of CaCp, CaMeCp, and CaPy are shown in Figures 1–10. The bandwidths in the excitation spectra of the features attributed to these molecules are on the order of 2.5 cm^{-1} while those in the dispersed fluorescence spectra are ~6 cm^{-1}. In addition to the CaCp, CaMeCp, and CaPy radicals, CaH is also formed, as is evident from the presence of the two spin–orbit components of the CaH $A^2\Pi$–$X^2\Sigma^+$ 0–0 transitions (spin–orbit splitting of 80 cm^{-1} in the excited state) that can be seen, for example, in Figure 1.

In the case of CaMeCp, its excitation spectrum (Figure 5) shows that CaCp and $CaCH_3$ are also formed during the reaction. There are two likely main sources of the $CaCH_3$ radicals. (i) Presumably, laser photolysis of $C_5H_5CH_3$ also yields a small amount of CH_3 radicals which can then compete with MeCp in reacting with the metal atoms. (ii) Laser vaporization of the Ca rod produces metal atoms in their ground (^1S) and metastable excited (^3P) states. Metal atoms in their ^3P states can then insert themselves between the Cp ring and the CH_3 group giving rise to both CaCp and $CaCH_3$. This should not come as a surprise because, in fact, the insertion mechanism is the main source of radicals in the Broida oven technique.[12] In Figure 5, the two spin–orbit components of the $\tilde{A}^2E$–$\tilde{X}^2A_1$ 0_0^0 transition of $CaCH_3$ are observed at 14703 and 14773 cm^{-1}.[10,11,14] The CaCp signal in Figure 5 is also at least in part a result of cracking the methylcyclopentadiene dimer, which according to refs 24 and 25 also produces a small amount of C_5H_6 (the Cp precursor).

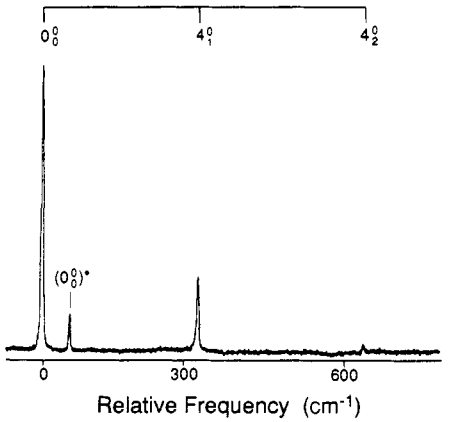

Figure 4. Dispersed fluorescence spectrum of CaCp obtained by pumping the $\tilde{A}^2E_{1(3/2)}$–$\tilde{X}^2A_1$ 0_0^0 band at 14564 cm^{-1}. The spectral resolution of the monochromator in this region is ~6 cm^{-1}. In addition to the series of bands originating from emission from the 0^0 vibrational level of the second spin–orbit component of the $\tilde{A}$ state, $^2E_{1(3/2)}$, a weak band (marked 0_0^0)*) can be seen approximately 56 cm^{-1} to the red of the pump frequency, which is due to emission from the 0^0 level of the first spin–orbit component of the $\tilde{A}$ state, $^2E_{1(1/2)}$, this level being populated by collisional relaxation.

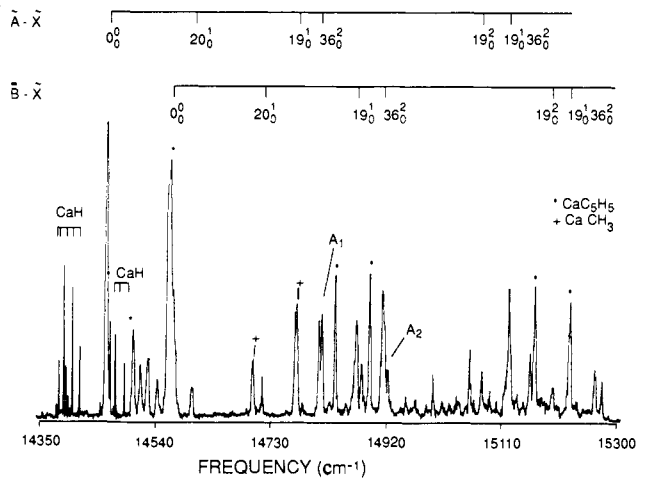

Figure 5. Laser excitation spectrum of CaMeCp. In addition to the CaMeCp vibronic bands, CaH, $CaCH_3$, and CaC_5H_5 features are seen here. See text for details on how these extra features arise.

In the remainder of this section, we will discuss first the electronic structure of these Ca-containing radicals. This will be followed by the assignment of vibrational structure observed in their electronic spectra. In the case of CaMeCp, very low-frequency bands attributed to transitions involving internal rotation of the methyl group will also be addressed in the final section.

A. Electronic Structure. 1. CaCp. The electronic structure of CaCp has been described previously by O'Brien and Bernath,[8] and later, a consistent picture was provided by ab initio electron propagator calculations performed by Ortiz.[26] Briefly, the ground and low-lying excited electronic states of CaCp are considered to be strongly ionic, correlating with electronic states of the separated ionic entities, Ca^+ and Cp^- ($\tilde{X}^1A_1'$). Cp^- is a closed-shell

(24) Richardson, J. H.; Stephenson, L. M.; Brauman, J. I. *J. Chem. Phys.* **1973**, *59*, 5068.
(25) Csicsery, S. M. *J. Org. Chem.* **1960**, *25*, 518.
(26) Ortiz, J. V. *J. Am. Chem. Soc.* **1991**, *113*, 3593.
(27) Haiduc, I.; Zuckerman, J. J. *Basic Organometallic Chemistry*; Walter de Gruyter: Berlin, 1985.

Table I. Transition Frequencies[a] for the CaCp Excitation Spectrum

	assignment[b]			
frequency[c]	$\tilde{A}^2E_{1(1/2)}$–$\tilde{X}^2A_1$	$\Delta\nu$[d]	$\tilde{A}^2E_{1(3/2)}$–$\tilde{X}^2A_1$	$\Delta\nu$[d]
14 508 vs	0_0^0	0		
14 564 vs			0_0^0	0
14 827 w	A	319		
14 837 vs	4_0^1	329		
14 893 s			4_0^1	329
14 952 m	10_0^2	444		
14 995 m			10_0^2	431
15 055 m	B_1	547		
15 117 m			B_2	553
15 133 m	C_1	625		
15 162 s	4_0^2	654		
15 197 m			C_2	633
15 218 s			4_0^2	654
15 246 m	3_0^1	738		
15 311 m			3_0^1	747
15 377 m	15_0^1	869		
15 426 m			15_0^1	862
15 486 m	4_0^3	978		
15 536 m			4_0^3	972
15 547 m	13_0^1	1039		
15 599 m			13_0^1	1035

[a] In cm^{-1}. [b] ν_2 is the a_1 CC stretch, ν_3 is the a_1 CH wag, ν_4 is the a_1 Ca–Cp stretch, ν_{10} is the e_1 Ca–Cp bend, ν_{13} is the e_2 CH deformation, and ν_{15} is the e_2 CH wag. No assignment has been made for bands labeled A–C. [c] To help the reader identify particular bands in the excitation spectrum, we use the following labels after each frequency to indicate the approximate intensity of a band: vs = very strong, s = strong, m = medium, and w = weak. [d] Frequency relative to the origin band (cm^{-1}).

Table II. Transition Frequencies[a] for the d_5-CaCp Excitation Spectrum

	assignment[b]			
frequency[c]	$\tilde{A}^2E_{1(1/2)}$–$\tilde{X}^2A_1$	$\Delta\nu$[d]	$\tilde{A}^2E_{1(3/2)}$–$\tilde{X}^2A_1$	$\Delta\nu$[d]
14 508 vs	0_0^0	0		
14 564 vs			0_0^0	0
14 824 s	4_0^1	316		
14 880 s			4_0^1	316
14 949 m	10_0^2	441		
14 992 w			10_0^2	428
15 020 w	3_0^1	512		
15 085 w			3_0^1	521
15 122 m	15_0^1	614		
15 139 m	4_0^2	631		
15 185 w			15_0^1	621
15 198 m			4_0^2	634
15 235 m	13_0^1	727		
15 313 m			13_0^1	749
15 323 m	A_1	815		
15 400 m			A_2	836
15 457 m	4_0^3	949		

[a] In cm^{-1}. [b] ν_2 is the a_1 CC stretch, ν_3 is the a_1 CH wag, ν_4 is the a_1 Ca–Cp stretch, ν_{10} is the e_1 Ca–Cp bend, ν_{13} is the e_2 CH deformation, and ν_{15} is the e_2 CH wag. No assignment has been made for bands labeled A. [c] To help the reader identify particular bands in the excitation spectrum, we use the following labels after each frequency to indicate the approximate intensity of a band: vs = very strong, s = strong, m = medium, and w = weak. [d] Frequency relative to the origin band (cm^{-1}).

aromatic ion, whose added stability enhances the ionic nature of the Ca–Cp bond. The molecular orbitals of CaCp of importance in the observed electronic transition can be treated, to a first approximation, as the orbitals of the Ca^+ ion being perturbed by the Cp^- ligand. The equilibrium geometry of CaCp consists of the Ca^+ ion sitting above the center of the Cp^- ring (η^5-bonding[20]), and therefore CaCp belongs under C_{5v} point group symmetry. Under this point group, the valence Ca^+ atomic orbitals transform as 4s → a_1, 3d → $a_1 + e_1 + e_2$, and 4p → $a_1 + e_1$. In the ground $\tilde{X}^2A_1$ state of CaCp, the unpaired electron is essentially located in a Ca^+ 4s atomic orbital which has a small admixture of $4p_z$ character. Excitation of the unpaired electron to e_1 or a_1 molecular orbitals (MO) of mixed Ca^+ 3d/4p character results in the formation of the $\tilde{A}^2E_1$ and $\tilde{B}^2A_1$ excited electronic states of CaCp. As described by O'Brien and Bernath,[8] this model explains the main features of the electronic spectra of CaCp.

Following O'Brien and Bernath, we assign the bands at 14 508 and 14 564 cm^{-1} in the excitation spectrum of CaCp (Figure 1 and Table I) as the origin bands of the $\tilde{A}^2E_{1(1/2)}$–$\tilde{X}^2A_1$ and $\tilde{A}^2E_{1(3/2)}$–$\tilde{X}^2A_1$ transitions, respectively. The splitting of 56 cm^{-1} between the two strongest features in the excitation spectrum is unequivocably assigned as the spin–orbit splitting in the $\tilde{A}^2E_1$ state of CaCp as indicated above the spectrum in Figure 1 since a similar doubling is also observed for other vibronic components in the $\tilde{A}$–$\tilde{X}$ system. Given that the atomic spin–orbit parameter for Ca^+ 3d, ζ_{3d}, is 24 cm^{-1} and that of Ca^+ 4p, ζ_{4p}, is 148 cm^{-1},[28] then the observed spin–orbit splitting in CaCp is entirely consistent with the idea that the unpaired electron in the $\tilde{A}^2E_1$ state of CaCp is residing in an MO which is primarily a 3d/4p mixture in character and that the Ca–Cp bond is predominantly ionic. Furthermore, the observation of spin–orbit splitting in the $\tilde{A}^2E_1$ state of CaCp is firm evidence that Ca^+ is indeed ring-bonded with C_{5v} point group symmetry. For any other reasonable geometry (e.g., η^1-, η^2-, or η^3-bonding), no electronic state degeneracy would be possible.

The excitation spectrum of d_5-CaCp is shown in Figure 2. The origin bands of the two spin–orbit components of the $\tilde{A}$–$\tilde{X}$ transition remain at 14 508 and 14 564 cm^{-1} (Table II). As expected, full deuteration of the Cp ring does not alter the magnitude of the spin–orbit splitting in the $\tilde{A}$ state.

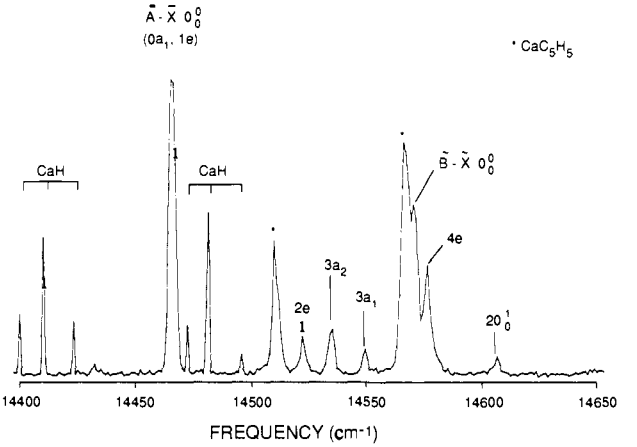

Figure 6. An expanded portion of the excitation spectrum of CaMeCp near the $\tilde{A}$–$\tilde{X}$ origin band showing methyl torsional features. The torsional bands are labeled by the excited-state torsional levels only.

2. CaMeCp. In going from CaCp to CaMeCp, one of the hydrogen atoms on the cyclopentadienyl ring is replaced by a methyl group. Despite this methyl substitution, one would not expect the bonding between calcium and the organic substrate to be significantly altered. In other words, we expect the Ca^+ ion to be located also above the $MeCp^-$ ring in an η^5-bonding fashion. In going from CaCp to CaMeCp, the overall symmetry of the molecule is lowered from C_{5v} to C_s (assuming that the methyl group is a structureless ball). However, there should be a direct correlation between the electronic states of the two molecules. Thus the $\tilde{X}^2A_1$ and $\tilde{B}^2A_1$ electronic states of CaCp correlate with the $\tilde{X}^2A'$ and $\tilde{C}^2A'$ electronic states in CaMeCp while the lower symmetry in CaMeCp splits the $\tilde{A}^2E_1$ state in CaCp into two distinct states of CaMeCp having symmetries of $^2A'$ and $^2A''$.

Armed with this simple model, we can assign the CaMeCp bands in the excitation spectrum in Figure 5 to two electronic band systems, the $\tilde{A}$–$\tilde{X}$ and $\tilde{B}$–$\tilde{X}$ systems. We assign the strong band at 14 465 cm^{-1} (Table III) as the $\tilde{A}$–$\tilde{X}$ 0_0^0 band since scans further to the red of this feature revealed no other bands which can be attributed to CaMeCp. There is a second strong band, that with

(28) Moore, C. E. *Atomic Energy Levels as Derived from the Analyses of Optical Spectra*; National Bureau of Standards Circulation No. 467; U.S. Government Printing Office: Washington, DC, 1952.

Table III. Transition Frequencies[a] for CaMeCp $\tilde{A}$–$\tilde{X}$ and $\tilde{B}$–$\tilde{X}$ Excitation Spectra

	assignment[b]				
	$\tilde{A}$–$\tilde{X}$			$\tilde{B}$–$\tilde{X}$	
frequency[c]			$\Delta\nu$[d]		$\Delta\nu$[d]
14 465 vs	0_0^0	$0a_1$, 1e	0		
14 520 m		2e	55		
14 532 m		$3a_2$	67		
14 547 m		$3a_1$	82		
14 567 s				0_0^0	0
14 573 m		4e	108		
14 604 m	20_0^1		139		
14 717 m				20_0^1	150
14 772 m	19_0^1	$0a_1$, 1e	307		
14 814 m	36_0^2		349		
14 817 m	A_1		352		
14 827 w	19_0^1	2e	362		
14 840 w	19_0^1	$3a_2$	375		
14 854 w	19_0^1	$3a_1$	389		
14 866 w				20_0^2	299
14 871 m				19_0^1	304
14 880 w	19_0^1	4e	415		
14 913 w	$19_0^1 20_0^1$		448		
14 917 m				36_0^2	350
14 923 w				A_2	356
15 079 w	19_0^2		614		
15 119 m	$19_0^1 36_0^2$		654		
15 176 w				19_0^2	609
15 220 m				$19_0^1 36_0^2$	653

[a] In cm^{-1}. [b] The notation employed for labeling the skeletal vibrations is the following: ν_{19} for the metal–ligand stretch, ν_{20} for the symmetric metal–ligand bend, and ν_{36} for the asymmetric metal–ligand bend. Torsional bands are labeled according to the symmetry of the excited state torsional level. Band A is still unassigned. [c] Intensity labels: vs = very strong, s = strong, m = medium, w = weak. [d] Frequency relative to the origin band.

a maximum at 14 565 cm^{-1}, which is actually composed of the $\tilde{B}$–$\tilde{X}$ 0_0^0 band (at 14 567 cm^{-1}) and two other bands. To illustrate this, we show in Figure 6 an expanded portion of the excitation spectrum of CaMeCp near the two origin bands, and indeed three distinct bands are clearly seen in the 14 560–14 575 cm^{-1} region. The band at 14 564 cm^{-1}, which is marked with an asterisk, is the CaCp $\tilde{A}^2E_{1(3/2)}$–$\tilde{X}^2A_1$ 0_0^0 band. The highest frequency number of the group of three peaks, that at 14 573 cm^{-1}, is tentatively attributed to a methyl torsional transition (see section IIIC). Assignment of the bands at 14 508 and 14 564 cm^{-1} to the two spin–orbit components of the CaCp $\tilde{A}$–$\tilde{X}$ 0_0^0 transition is verified by their transition frequencies and by the dispersed fluorescence spectra obtained by pumping these bands. However, if one disperses the fluorescence by fixing the dye laser frequency to 14 567 cm^{-1}, which is the frequency corresponding to the central band of the three-band cluster in the 14 560–14 575-cm^{-1} region, the intensity distribution of the vibrational structure is almost identical to that obtained by pumping the $\tilde{A}$–$\tilde{X}$ 0_0^0 band of CaMeCp (compare Figure 7a and b) and very different from that of CaCp (see Figure 4). This indicates that the 14 567-cm^{-1} band is not due to excitation of a vibration in the $\tilde{A}$ state but instead is more likely due to $\tilde{B}$–$\tilde{X}$ 0_0^0 band. If correct, the energy separation between the $\tilde{A}$–$\tilde{X}$ and $\tilde{B}$–$\tilde{X}$ origin bands is only 102 cm^{-1}.

As far as the $\tilde{C}$–$\tilde{X}$ band system of CaMeCp (which correlates with the $\tilde{B}$–$\tilde{X}$ system of CaCp) is concerned, we have scanned to frequencies as high as 17 000 cm^{-1} without seeing any clear evidence of this system. It is quite possible that the $\tilde{C}$–$\tilde{X}$ band system lies outside of the region scanned or it may be obscured by vibronic bands of CaCp.

3. CaPy. The electronic structure of CaPy is believed to closely resemble that of CaCp, as discussed by Bopegedera et al.[9] Thus, the bonding will be mainly ionic, and the electronic states will correlate with separated ionic entities, $Ca^+ + Py^-$. Py^- is a heterocyclic ligand isoelectronic with the carbocyclic ligand, Cp^-, and is therefore also a highly stable aromatic ring system.

There are two most likely binding sites for the metal atom in an MPy molecule such as CaPy.[9,17] The two possibilities are (i) N-bonding (η^1-bonding), where the Ca atom is bonded directly to the N atom in the plane of the ring, paralleling the case of $CaNH_2$.[29,30] If this η^1-bonding scheme is valid, this would mean that CaPy has C_{2v} point group symmetry. (ii) The other possibility is ring-bonding (η^5), where the metal atom is located above the ring analogous to the case of CaCp. As will be shown shortly, the electronic spectra support the ring-bonding scheme in CaPy, giving this molecule C_s symmetry.

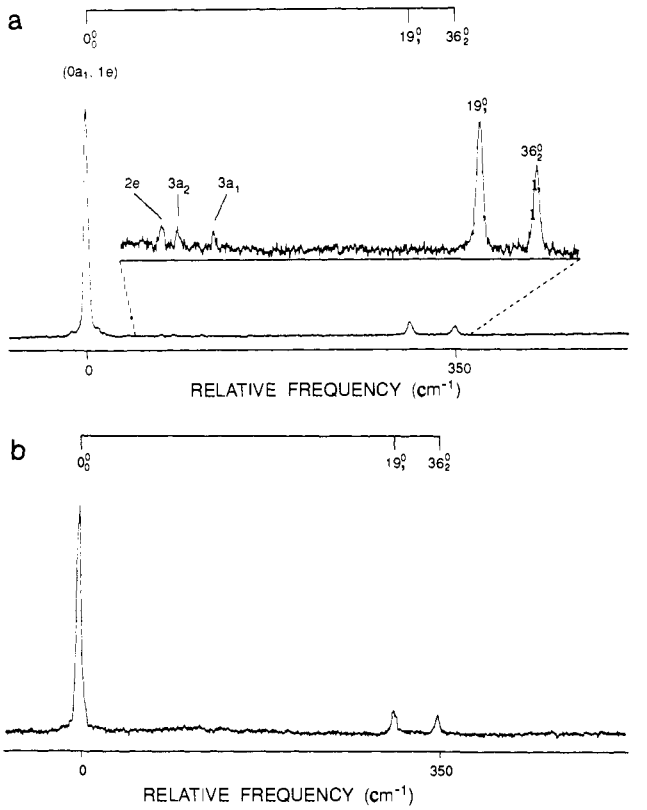

Figure 7. Dispersed fluorescence spectra of CaMeCp obtained by pumping (a) the $\tilde{A}$–$\tilde{X}$ 0_0^0 band at 14 465 cm^{-1} (b) the $\tilde{B}$–$\tilde{X}$ 0_0^0 band at 14 567 cm^{-1}. A magnified view of a part of the spectrum in Figure 7a shows the torsional features present in the spectrum. The torsional bands are labeled by the ground electronic state torsional levels. Note that some scattered light contributes to the intensity at the pump position. See text for details.

As in CaCp, the electronic transitions observed for CaPy are presumably essentially metal-centered. According to Bopegedera et al.,[9] the Ca^+ ion in CaPy experiences a pseudo-C_{5v} environment, i.e., the Ca^+ ion is located above the approximate center of the Py^- ring and is not significantly perturbed by the substitution of a N atom for a CH group in passing from CaCp to CaPy. According to this model, the degeneracies of the orbitals of Ca^+ are retained even though the actual point group symmetry is C_s for CaPy.

In Figure 8, we show the excitation spectrum of jet-cooled CaPy. The $\tilde{A}$–$\tilde{X}$ electronic origin at 14 324 cm^{-1} and some 68 cm^{-1} to the blue is a stronger band which we attribute to the $\tilde{B}$–$\tilde{X}$ 0_0^0 transition. Built upon each of these origins are a number of vibrational features identified in Figure 8. A third electronic band system whose origin is at 14 731 cm^{-1} is also observed in Figure 8, which is assigned to the $\tilde{C}$–$\tilde{X}$ band system. According to Bopegedera et al.,[9] the excited electronic states, which we identify in the present work as the $\tilde{A}$ and $\tilde{B}$ states, are due to the two spin–orbit components of a $^2E_1$ excited state (using C_{5v} notation). This is certainly a tempting assignment since the so-called $\tilde{A}$–$\tilde{X}$ and $\tilde{B}$–$\tilde{X}$ 0_0^0 bands in Figure 8 are separated by 68 cm^{-1}, a spacing which is reasonably similar to the spin–orbit splitting of 56 cm^{-1} found for the $\tilde{A}^2E_1$ state of CaCp. Furthermore, the $\tilde{A}$–$\tilde{X}$ and

(29) Bopegedera, A. M. R. P.; Brazier, C. R.; Bernath, P. F. *J. Phys. Chem.* **1987**, *91*, 2779.
(30) Whitham, C. J.; Jungen, C. *J. Chem. Phys.* **1990**, *93*, 1001.

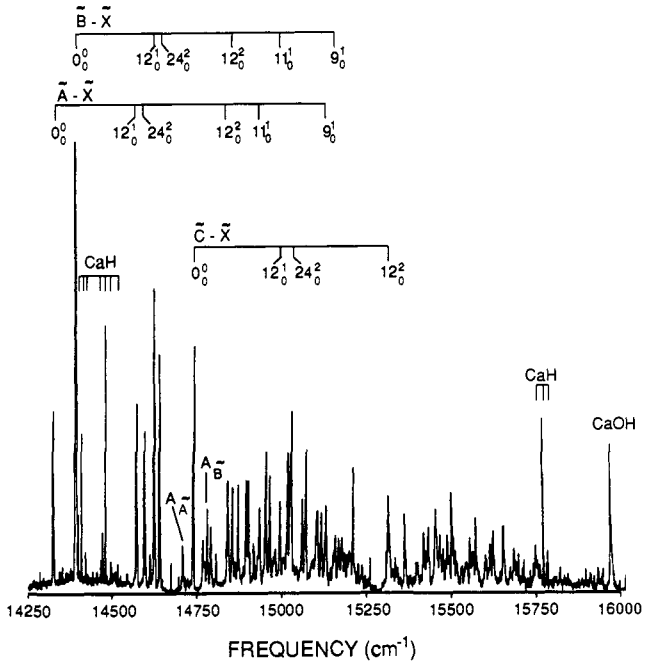

Figure 8. Laser excitation spectrum of CaPy. This spectrum is shown with no corrections for variations in dye laser intensity as a function of wavelength. As is very evident in this trace, three different dye solutions were used when this spectrum was recorded.

Table IV. Transition Frequencies[a] for the CaPy Excitation Spectrum

	assignment[b]					
frequency[c]	$\tilde{A}$–$\tilde{X}$	$\Delta\nu^d$	$\tilde{B}$–$\tilde{X}$	$\Delta\nu^d$	$\tilde{C}$–$\tilde{X}$	$\Delta\nu^d$
14324 s	0_0^0	0				
14392 vs			0_0^0	0		
14572 s	12_0^1	248				
14595 m	24_0^2	271				
14623 s			12_0^1	231		
14639 s			24_0^2	247		
14702 m	$A_{\tilde{A}}$	378				
14731 s					0_0^0	0
14772 m			$A_{\tilde{B}}$	380		
14833 m	12_0^2	509				
14847 m	$12_0^1 24_0^2$	523				
14855 m			12_0^2	463		
14864 m	24_0^4	540	$12_0^1 24_0^2$	472		
14888 m			24_0^4	496		
14922 m	11_0^1	598				
14946 m	$A_{\tilde{A}} + 12_0^1$	622				
14973 w	$A_{\tilde{A}} + 24_0^2$	649				
14987 m			11_0^1	595		
14999 m			$A_{\tilde{B}} + 12_0^1$	607		
15009 m			$A_{\tilde{B}} + 24_0^2$	617		
15020 s					12_0^1	289
15063 m					24_0^2	332
15096 m	$12_0^2 24_0^2$	772				
15121 m	9_0^1	797				
15145 m			9_0^1	753		
15298 m					12_0^2	567
15345 m					$12_0^1 24_0^2$	614
15399 w					24_0^4	668

[a] In cm^{-1}. [b] ν_9 is the a′ CH wag, ν_{11} is the a′ ring torsion, ν_{12} is the a′ Ca–Py stretch and ν_{24} is the a″ Ca–Py bend. Note that there are still several bands in Figure 8 which have not been assigned, e.g., band A. [c] To help the reader identify particular bands in the excitation spectrum, we use the following labels after each frequency to indicate the approximate intensity of a band: vs = very strong, s = strong, m = medium, and w = weak. [d] Frequency relative to the origin band (cm^{-1}).

$\tilde{B}$–$\tilde{X}$ band systems appear to possess rather similar vibrational structure.

However, on closer examination of Figure 8 and Table IV, the vibrational intervals observed for the $\tilde{A}$–$\tilde{X}$ and $\tilde{B}$–$\tilde{X}$ band systems

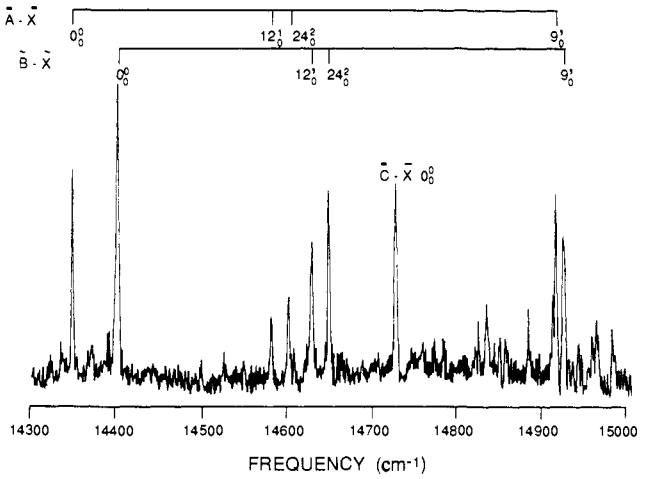

Figure 9. A portion of the laser excitation spectrum of d_4-CaPy.

Table V. Transition Frequencies[a] for the d_4-CaPy Excitation Spectrum

	assignment[b]					
frequency[c]	$\tilde{A}$–$\tilde{X}$	$\Delta\nu^d$	$\tilde{B}$–$\tilde{X}$	$\Delta\nu^d$	$\tilde{C}$–$\tilde{X}$	$\Delta\nu^d$
14349 m	0_0^0	0				
14402 s			0_0^0	0		
14581 m	12_0^1	232				
14602 m	24_0^2	253				
14628 s			12_0^1	226		
14648 s			24_0^2	246		
14729 s					0_0^0	0
14836 m	$12_0^1 24_0^2$	487	12_0^2	434		
14886 m			24_0^4	484		
14915 m	9_0^1	566				
14926 m			9_0^1	524		
15019 m					12_0^1	290
15041 m					24_0^2	312

[a] In cm^{-1}. [b] ν_9 is the a′ CH wag, ν_{11} is the a′ ring torsion, ν_{12} is the a′ Ca–Py stretch and ν_{24} is the a″ Ca–Py bend. Note that there are still several bands in Figure 9 which have not been assigned, e.g., band A. [c] To help the reader identify particular bands in the excitation spectrum, we use the following labels after each frequency to indicate the approximate intensity of a band: vs = very strong, s = strong, m = medium, and w = weak. [d] Frequency relative to the origin band (cm^{-1}).

are found to be significantly different. For example, for the progression in ν_{12}, which as discussed later is the Ca–Py stretching mode, the vibrational frequency in the $\tilde{A}$ state is measured as 248 cm^{-1} whereas that of the $\tilde{B}$ state is 231 cm^{-1}. The difference in frequencies of 17 cm^{-1} may be compared with the case of the $\tilde{A}^2E_1$ state of CaCp where there is no observed difference in the Ca–Cp stretching vibrational frequencies (329 cm^{-1}) for the $^2E_{1(1/2)}$ and $^2E_{1(3/2)}$ spin–orbit components. This comparison would seem to indicate that the 68-cm^{-1} "doubling" observed for CaPy is not due to pure spin–orbit splitting in the first excited electronic state. This is supported by the recording of the laser excitation spectrum of fully-deuterated d_4-CaPy (see Figure 9). If the doubling is due to spin–orbit splitting alone, no change in the magnitude of the splitting would be expected on deuteration (as observed in the case of fully-deuterated d_5-CaCp (see Tables I and II)). However, as can be seen from Table V, the splitting is reduced from 68 to 53 cm^{-1} on full deuteration of CaPy, which indicates that the $\tilde{A}$ and $\tilde{B}$ states have significantly different zero point vibrational energies for vibrations involving motion of the deuterium atoms.

Consequently, we identify the $\tilde{A}$ and $\tilde{B}$ states of CaPy as being distinct electronic states correlating with the $\tilde{A}^2E_1$ state of CaCp. We have insufficient evidence to determine which of these states is the $^2A'$ state and which is the $^2A''$ state. We can, however, attribute $^2A'$ symmetries to the $\tilde{X}$ and $\tilde{C}$ states of CaPy.

B. Vibrational Analysis. 1. CaCp. A schematic illustration of the 27 vibrational modes in a metal monocyclopentadienyl molecule with a general formula of MC_5H_5 and an assumed

equilibrium point group symmetry of C_{5v} was given in ref 15. Briefly, we can divide the 27 vibrational modes into two groups, metal–ring and intra-ring modes. The former group of modes, which involve motion of the metal atom with respect to the ring, are commonly referred to as skeletal modes. Not all of these modes are expected to be excited in the excitation and dispersed fluorescence spectra of CaCp. From symmetry arguments, only the totally symmetric (a_1) modes, namely, ν_1 (CH stretch), ν_2 (CC stretch), ν_3 (CH wag), and ν_4 (metal–ring stretch), would be expected to yield the major features observed in the spectra in the absence of any vibronic coupling mechanisms. Estimates of the frequencies of these and other modes in CaCp can be obtained from the frequencies of analogous modes in $CaCp_2$ and in other metallocenes (see ref 15 for a summary). This is extremely useful information for making vibrational assignments, particularly with regard to intra-ring modes.

(a) Skeletal Modes. Laser excitation and dispersed fluorescence spectra of CaCp are shown in Figures 1–4. As mentioned earlier, a number of identifiable vibrational progressions originate from each of the origin bands of the two spin–orbit components which are separated by 56 cm^{-1}. We follow the original assignment of O'Brien and Bernath[8] and attribute the most prominent progression in Figure 1 as being due to excitation of the metal–ligand stretch, ν_4. For example, in Figure 1 and Table I, we assign the bands at 14837, 15162, and 15486 cm^{-1} as being, respectively, due to the 4_0^1, 4_0^2, and 4_0^3 transitions built upon the $\tilde{A}^2E_{1(1/2)}$–$\tilde{X}^2A_1$ 0_0^0 band. In both excited-state spin–orbit components, we obtain a frequency of 329 cm^{-1} for ν_4, which is in close agreement with that reported by O'Brien and Bernath[8] (325 cm^{-1}). We have also observed two bands of medium intensity, at 14952 and 14995 cm^{-1}, which are, respectively, 444 and 431 cm^{-1} to the blue of the origin bands of the two spin–orbit components. We tentatively assign these bands to the 10_0^2 transitions of the spin–orbit pair, ν_{10} being the doubly degenerate (e_1) Ca–Cp bending mode. This gives frequencies of 444 and 431 cm^{-1} for $2\nu_{10}$ in the $\tilde{A}^2E_{1(1/2)}$ and $\tilde{A}^2E_{1(3/2)}$ states, respectively.

For d_5-CaCp (Figure 2 and Table II), ν_4 is measured as 316 cm^{-1} for the $\tilde{A}$ state. This corresponds to a decrease in the frequency of ν_4 on full deuteration of 13 cm^{-1}, which is larger than the ~–5-cm^{-1} shift expected if the Ca–Cp molecule is treated as a pseudodiatomic harmonic oscillator. This may indicate some minor participation of the hydrogen atoms in the vibrational motion which constitutes ν_4. A much smaller decrease of 2 cm^{-1} is found for the Ca–Cp bending mode, i.e., $2\nu_{10}$, on full deuteration.

We have also recorded dispersed fluorescence spectra of CaCp by pumping the two spin–orbit components of the $\tilde{A}$–$\tilde{X}$ 0_0^0 transition. This provides us with information on the vibrations in the ground electronic state. In Figure 4, we show the spectrum obtained by dispersing the fluorescence following excitation of the $\tilde{A}^2E_{1(3/2)}$–$\tilde{X}^2A_1$ 0_0^0 transition. Little structure is seen in the spectrum. In fact, apart from a band due to emission from the 0^0 level of the $\tilde{A}^2E_{1(1/2)}$ state (populated by collisional relaxation from the $\tilde{A}^2E_{1(3/2)}$ 0^0 level), marked with an asterisk in Figure 4, the only other features to the red of the pump frequency are due to a vibrational progression in ν_4 in the ground electronic state. Our measured frequency of 311 cm^{-1} for ν_4 in the $\tilde{X}$ state is in good agreement with that reported in ref 8 of 312 cm^{-1}.

A summary of the frequencies determined for the skeletal modes ν_4 and $2\nu_{10}$ in the $\tilde{X}$ and $\tilde{A}$ electronic states of CaCp and d_5-CaCp is given in Table VI. For comparison purposes, this table also includes the corresponding skeletal vibrational frequencies of the full-sandwich compound, $CaCp_2$, obtained from an infrared study of solid $CaCp_2$. We note that the Ca–Cp stretching frequency in both ground and excited electronic states of CaCp is significantly larger than the Ca–Cp stretching frequency of 284 cm^{-1} in the ground electronic state of $CaCp_2$.[3] Furthermore, a clear increase in the ν_4 frequency is observed on $\tilde{A}$–$\tilde{X}$ excitation of CaCp, which implies that there is a strengthening of the Ca–Cp bond in going from the $\tilde{X}$ to the $\tilde{A}$ state. Unfortunately, the vibrational structure in the dispersed fluorescence spectrum of CaCp is not extensive enough to provide a reasonable estimate of the dissociation energy of the Ca–Cp bond in the $\tilde{X}$ state. However, that of the $\tilde{A}$ state can be estimated by employing a Birge–Sponer extrapolation of the three members of the ν_4 progression in the $\tilde{X}^2A_1$–$\tilde{A}^2E_{1(3/2)}$ band system. Assuming that the Ca–Cp potential is reasonably described by a Morse function, the Ca–Cp bond energy is ~10200 cm^{-1} in the $\tilde{A}$ state.

Table VI. Vibrational Frequencies[a] of CaCp, d_5-CaCp, and $CaCp_2$

	CaCp[b]			d_5-CaCp[b]		$CaCp_2$[c]
mode[d]	$\tilde{X}^2A_1$	$\tilde{A}^2E_{1(1/2)}$	$\tilde{A}^2E_{1(3/2)}$	$\tilde{A}^2E_{1(1/2)}$	$\tilde{A}^2E_{1(3/2)}$	$\tilde{X}$
ν_3	–	738	747	512	521	750
ν_4	311	329	329	316	316	284
$2\nu_{10}$	–	444	431	441	428	–
ν_{13}[e,f]	–	1039	1035	727	749	–
ν_{15}[f]	–	869	862	614	621	–

[a] In cm^{-1}. [b] This work. [c] Reference 3. [d] ν_3 is the a_1 CH wag, ν_4 is the a_1 Ca–Cp stretch, ν_{10} is the e_1 Ca–Cp bend, ν_{13} is the e_2 CH deformation, and ν_{15} is the e_2 CH wag. [e] Another possible assignment for this is ν_2. See text. [f] This assignment is tentative.

We have also simulated the intensity pattern of the ν_4 progression in the $\tilde{A}$–$\tilde{X}$ system assuming a pseudodiatomic treatment of the stretching of the Ca–Cp bond. Our Franck–Condon simulation suggests a decrease of ~0.08 Å in the Ca–Cp separation in going from the $\tilde{X}$ to the $\tilde{A}$ electronic state. The contraction in the metal–ligand distance is probably due in part to the fact that the $\tilde{A}$ state arises essentially from a Ca^+ 3d/4p hybrid molecular orbital. In the previous section, the bonding in CaCp is said to be mainly ionic in nature, with the unpaired electron located in an MO which is essentially metal in character. However, the bonding in CaCp will inevitably involve some degree of covalency. The shape of the metal 3d and 4p orbitals makes their overlap with the C2pπ orbitals on the ring more effective than that of the 4s orbitals, and this will enhance the covalent character of the CaCp bond and should contribute to the increase in bond strength on $\tilde{A}$–$\tilde{X}$ excitation.

(b) Intra-Ring Modes. There are a number of vibronic bands in the excitation spectrum of CaCp in Figure 1 which cannot be assigned to vibrational progressions in skeletal modes. We are fairly certain that these bands arise from vibrational excitation of CaCp and not some other molecule since they are not, for example, observed in the excitation spectrum of CaPy. We therefore ascribe these bands as being due to activity of intra-ring modes of CaCp.

Two such medium-intensity bands are those observed at 15246 and 15311 cm^{-1}, which are, respectively, 738 and 747 cm^{-1} from the respective origin bands of the $\tilde{A}$–$\tilde{X}$ spin–orbit pair. In the infrared spectrum of $CaCp_2$,[3] a band at 750 cm^{-1} was observed and assigned as ν_3 (a_1 CH wag) in the ground electronic state of $CaCp_2$. In light of this, we tentatively assign the bands of CaCp at 15246 (+738) and 15311 (+747) cm^{-1} to the $\tilde{A}^2E_{1(1/2)}$–$\tilde{X}^2A_1$ and $\tilde{A}^2E_{1(3/2)}$–$\tilde{X}^2A_1$ 3_0^1 transitions, respectively. Convincing experimental evidence in favor of these assignments comes from the excitation spectrum of d_5-CaCp (Figure 2). For d_5-CaCp, ν_3 is measured to be 512 ($\tilde{A}^2E_{1(1/2)}$) and 521 ($\tilde{A}^2E_{1(3/2)}$) cm^{-1}, which agrees well with the calculated frequencies of 521 and 528 cm^{-1}, respectively, assuming this mode involves essentially pure hydrogenic motion.

There are clearly a number of weak bands in the excitation spectrum of CaCp which cannot be assigned to the other two remaining a_1 intra-ring modes (ν_1 and ν_2) on the basis of their relative frequencies.[15] However, the $\tilde{A}$ state of CaCp is doubly degenerate and therefore is subject to Jahn–Teller distortion. (It must be pointed out that one would only expect a weak Jahn–Teller distortion in CaCp since the unpaired electron is essentially located in a metal-centered orbital in the $\tilde{A}^2E_1$ state.) Thus it is quite possible that some of the unassigned bands originate from single quantum excitation of Jahn–Teller active modes. Only modes having e_2 symmetry are potentially Jahn–Teller active under C_{5v} symmetry. For CaCp, these are the intra-ring modes ν_{11}–ν_{16}.[15] For example, the bands at 15055 (+547) and 15117 (+553) cm^{-1} (bands labeled as B_1 and B_2 in Figure 1) can be tentatively assigned to the $\tilde{A}^2E_{1(1/2)}$–$\tilde{X}^2A_1$ and $\tilde{A}^2E_{1(3/2)}$–$\tilde{X}^2A_1$ 16_0^1 transitions, respectively. We note that in similar Cp-containing compounds,[15]

the frequency of ν_{16} (ring torsion) ranges from 590 to 630 cm^{-1}. It is therefore also possible that the vibronic bands labeled as C_1 and C_2 at 15133 (+625) and 15197 (+633) cm^{-1} are due to 16_0^1. Unfortunately, we cannot unequivocably assign these bands on the basis of the limited spectroscopic data available in this study.

However, for the potentially Jahn–Teller active mode involving hydrogenic motion whose frequencies are expected to fall within our scan range, namely, ν_{13} (e_2 CH deformation) and ν_{15} (e_2 CH wag), we can employ the spectroscopic data for d_5-CaCp to examine possible single quantum excitation of these modes. From ref 15, ν_{13} and ν_{15} were found to have frequencies of ~1060 and ~800 cm^{-1}, respectively, for several nondeuterated MCp-containing compounds. Using these frequencies as a guide, we tentatively assign intervals of 1039 and 1035 cm^{-1} (see Table I) as ν_{13} in the $\tilde{A}^2E_{1(1/2)}$–$\tilde{X}^2A_1$ and $\tilde{A}^2E_{1(3/2)}$–$\tilde{X}^2A_1$ manifolds, respectively, (the 13_0^1 bands are labeled in Figure 1). However, it is also possible that these frequencies might be due to the totally symmetric CC stretch, ν_2, which has a frequency in the region of 1100 cm^{-1}.[15] If they are due to ν_{13}, then a decrease in frequency from ~1040 to ~735 cm^{-1} should result from deuteration of the Cp ring. This behavior is indeed observed on deuteration. As can be seen by inspecting Table II, two new bands are observed in the d_5-CaCp excitation spectrum, which are located 727 and 749 cm^{-1} from the $\tilde{A}^2E_{1(1/2)}$–$\tilde{X}^2A_1$ and $\tilde{A}^2E_{1(3/2)}$–$\tilde{X}^2A_1$ 0_0^0 transitions, respectively, and the original bands in nondeuterated CaCp at 15547 and 15599 cm^{-1} disappear. Hence we can be fairly certain that we are observing ν_{13}.

Following similar arguments, we have also obtained evidence for single quantum excitation of mode ν_{15}. We assign the bands corresponding to excited-state intervals of 869 and 862 cm^{-1} for the two spin–orbit components as being due to ν_{15}, since on deuteration, the intervals are reduced to 614 and 621 cm^{-1}. This is entirely consistent with a hydrogenic vibration.

In the dispersed fluoresence spectrum of CaCp shown in Figure 4, none of the observed bands can be attributed to excitation of intra-ring modes. Their absence can be ascribed to the fact that intra-ring modes are expected to be somewhat weaker than the skeletal modes from Franck–Condon considerations, as we can see from the excitation spectrum of CaCp. In view of the fact that the sensitivity of the detector used in the dispersed fluorescence experiments is relatively insensitive in the red region of the spectrum, it would therefore be expected to be difficult to observe intra-ring bands. This situation is exacerbated by the fact that most intra-ring modes have frequencies which are generally >600 cm^{-1}, which means that their bands are expected to be far to the red of the pump frequency, a region where our detector is almost nonfunctional.

A summary of the known vibrational frequencies of CaCp and d_5-CaCp is given in Table VI.

(c) "$\tilde{B}^2A_1$–$\tilde{X}^2A_1$" Band System of CaCp. Our discussion of the vibrational structure has so far been restricted to the $\tilde{A}$–$\tilde{X}$ manifold. It is interesting to note that O'Brien and Bernath also observed additional vibrational structure in their low-resolution study of CaCp,[8] which they attributed to the "$\tilde{B}^2A_1$–$\tilde{X}^2A_1$" band system. Although the actual spectrum was not shown in their report, three bands were apparently observed, one at 16772 cm^{-1} which they assigned as the $\tilde{B}$–$\tilde{X}$ 0_0^0 band, another at 17072 cm^{-1} assigned as the 4_0^1 band, and a third at 16470 cm^{-1} attributed to the 4_1^0 hot band. We have also scanned this region and show the excitation spectrum in Figure 3. The structure seen in this spectra, which is reproducible, is quite complex, and we have been unable to identify any clearly discernible pattern. Given the very much lower resolution in ref 8, the complex structure we observed could not have been resolved by O'Brien and Bernath. The cluster of features in the 16700–16850-cm^{-1} region were presumably observed as a single broad band in O'Brien and Bernath's spectrum. Consistent with this is the fact that the most intense band in Figure 3, that approximately in the center of the main cluster, is at 16765 cm^{-1}, which is close to the 16772 cm^{-1} claimed to be the $\tilde{B}$–$\tilde{X}$ origin by O'Brien and Bernath. A second cluster of bands in our spectrum can be identified in the region 17000–17150 cm^{-1}. This presumably corresponds to the feature at 17072 cm^{-1} identified by O'Brien and Bernath as the 4_0^1 band. In view of the more complex structure resolved in this work, the $\tilde{B}$–$\tilde{X}$ assignments made by O'Brien and Bernath must be regarded as being questionable. First of all, the large number of bands relatively close to the apparent $\tilde{B}$–$\tilde{X}$ electronic origin is difficult to explain in terms of skeletal and/or intra-ring modes since it would imply that there are several very low-frequency vibrational modes (i.e., $\nu \leq 150$ cm^{-1}) of CaCp. We have also considered the possibility that the complexity arises in part or mainly from sequence band structure, which would means that CaCp is vibrationally hot in our expansion. The fact that no significant sequence or hot band structure is observed for the $\tilde{A}$–$\tilde{X}$ system would seem to rule out this possibility.

We are, however, fairly certain that these features are of CaCp in origin, for two main reasons. First, this band system was recorded by O'Brien and Bernath using the Broida oven technique. In a Broida oven, one would not expect any side products apart from CaH, a molecule which is known not to have any vibronic transition in this region. (In contrast, in our laser vaporization/photolysis technique, there is always the possibility of producing side products from photolysis of the organic precursor.) Second, the vibrational structure in Figure 3 disappears when cyclopentadiene was removed from or when pyrrole was introduced into the expansion.

We are therefore currently unable to assign the structure in the "$\tilde{B}$–$\tilde{X}$" band system. However, from the complexity of the vibrational structure in Figure 3, it is more likely that not one of these features is the actual $\tilde{B}$–$\tilde{X}$ origin band. Quite possibly, these bands arise from excitation from the vibrationless level in the ground state to some higher levels in the vibrational manifold of the $\tilde{B}$ state. If this is indeed the case, then it would mean that there is a significant geometry change on $\tilde{B}$–$\tilde{X}$ excitation for the actual origin band not to be observed.

2. CaMeCp. There are 36 normal modes of vibration for an MMeCp molecule such as CaMeCp.[18] Three are so-called skeletal modes while the remaining modes can be described as essentially ring-localized vibrations, i.e., intra-ring vibrations and modes involving motion of the methyl group (excluding methyl torsions).

(a) Skeletal Modes. Among the three skeletal modes, two are totally symmetric (a′), the metal-ring stretch (ν_{19}) and one of the two metal–ring bends (ν_{20}), assuming that the metal is ring-bonded. The a′ bending mode, ν_{20}, involves bending motion of the metal toward and away from the methyl group in the plane of symmetry of the molecule. The other metal–ring bending vibration, ν_{36}, is asymmetric (a″) and involves bending motion of the metal in a direction perpendicular to the symmetry plane.

In the excitation spectrum of CaMeCp (Figure 5), we have only been able to clearly identify excitation of the three skeletal modes of CaMeCp in the $\tilde{A}$–$\tilde{X}$ and $\tilde{B}$–$\tilde{X}$ band systems. In the $\tilde{A}^2E_1$ state of CaCp, the Ca–Cp stretching frequency is measured to be 329 cm^{-1}. Assuming that the force constant is unchanged, the corresponding increase in ring mass should result in a slight decrease in the Ca–ring stretching frequency in going from CaCp to CaMeCp. We therefore assign the medium-intensity bands at 14772 and 14871 cm^{-1} as being the 19_0^1 transitions for the $\tilde{A}$–$\tilde{X}$ and $\tilde{B}$–$\tilde{X}$ band systems, respectively, of CaMeCp. This gives frequencies of 307 and 304 cm^{-1} for ν_{19} for the $\tilde{A}$ and $\tilde{B}$ states of CaMeCp, respectively. Notice also that the $\tilde{A}$–$\tilde{X}$ 19_0^1 band is broader than most of the bands in Figure 5. This is attributed to the fact that the $\tilde{A}^2E_{3/2}$–$\tilde{X}^2A_1$ 0_0^0 band of $CaCH_3$ at 14773 cm^{-1} overlaps with the $\tilde{A}$–$\tilde{X}$ 19_0^1 band of CaMeCp. Furthermore, there are several bands at very much lower frequencies. Most of these features are attributed to methyl torsional transitions in the $\tilde{A}$–$\tilde{X}$ manifold (see section C) with the exception of the band at 14604 cm^{-1}, which we assign as the fully-allowed $\tilde{A}$–$\tilde{X}$ 20_0^1 transition. For the $\tilde{B}$–$\tilde{X}$ system, the band at 14717 cm^{-1} is tentatively assigned as the $\tilde{B}$–$\tilde{X}$ 20_0^1 transition. As summarized in Table VII, the ν_{20} frequencies are 139 and 150 cm^{-1} for the $\tilde{A}$ and $\tilde{B}$ states, respectively. The only skeletal mode which has so far not been mentioned in the assignment is the asymmetric Ca–MeCp bend, ν_{36}. Due to its symmetry (a″), only even quanta excitation of this mode is expected. Furthermore, its frequency is likely to be

Table VII. Vibrational Frequencies[a] of CaMeCp

mode[b]	$\tilde{X}$	$\tilde{A}$	$\tilde{B}$
ν_{19}	297	307	304
ν_{20}	143	139	150
$2\nu_{36}$	337	349	350

[a] In cm^{-1}. [b] ν_{19} for the metal–ligand stretch, ν_{20} for the symmetric metal–ligand bend, and ν_{36} for the asymmetric metal–ligand bend.

approximately twice that of ν_{20}. Indeed, two bands are observed with the approximately correct frequencies for this criterion, namely, those at 14814 (+349) and 14917 (+350) cm^{-1}. We therefore tentatively assign these as, respectively, the $\tilde{A}$–$\tilde{X}$ and $\tilde{B}$–$\tilde{X}$ 36_0^2 bands. Notice, however, that the intensities of the 36_0^2 bands are comparable to those of the 19_0^1 bands. Presumably, their unusual intensities are derived from a very strong Fermi resonance interaction between ν_{19} and $2\nu_{36}$.

Turning our attention now to the dispersed fluorescence spectra of CaMeCp, when the $\tilde{A}$–$\tilde{X}$ and $\tilde{B}$–$\tilde{X}$ 0_0^0 transitions are excited (Figure 7), only three bands are clearly seen which correspond to emission from the vibrationless level (0^0) in the $\tilde{A}$ or $\tilde{B}$ state to the 0_0, 19_1, and 36_2 vibrational levels in the ground electronic state. Thus, ν_{19} and $2\nu_{36}$ in the ground state are determined to be 297 and 337 cm^{-1}, respectively. The frequency of the metal–ring stretch, ν_{19} (297 cm^{-1}), in the CaMeCp ground state is clearly similar in magnitude to the measured Ca–ring stretch in CaCp of 311 cm^{-1} in its ground state. We have also pumped the $\tilde{A}$–$\tilde{X}$ 20_0^1 transition of CaMeCp (at 14604 cm^{-1}) and have found that the majority of the fluorescence is concentrated into a new band 143 cm^{-1} to the red of the pump position. This frequency does not fit any of the calculated methyl torsional levels in the ground electronic state of CaMeCp (section C) in the same way the 14604-cm^{-1} band does not fit any of the calculated $\tilde{A}$–$\tilde{X}$ methyl torsional transitions. From Franck–Condon arguments, we assign the 143-cm^{-1} spacing in the dispersed fluorescence spectrum as arising from excitation of ν_{20} in the $\tilde{X}$ state of CaMeCp.

(b) Intra-Ring and CH_3–Ring Vibrations. As far as the intra-ring and CH_3–ring (excluding methyl torsion) vibrations are concerned, there are several weak features in Figure 5 which have not been assigned and which may arise from these modes. For example, the bands labeled as A_1 and A_2 are, respectively, 352 and 356 cm^{-1} from the $\tilde{A}$–$\tilde{X}$ and $\tilde{B}$–$\tilde{X}$ 0_0^0 bands. It should be pointed out that similar relatively low-frequency bands were observed in the spectra of ZnMeCp and CdMeCp, the corresponding vibrational frequencies for these molecules being in the region of 300 cm^{-1}.[18] Paralleling our assignment for ZnMeCp and CdMeCp, it is quite possible that bands A_1 and A_2 are due to excitation of the symmetric C–CH_3 "out-of-plane" deformation.

A summary of the measured vibrational frequencies of CaMeCp in the $\tilde{X}$, $\tilde{A}$, and $\tilde{B}$ electronic states is given in Table VII.

3. CaPy. (a) Skeletal Modes. Paralleling the case of CaMeCp, there are three skeletal modes for CaPy, namely, the metal–ligand stretch (ν_{12}) and two bending modes (ν_{13} and ν_{24}).[9] Notice that we are using a different mode numbering system here than in CaMeCp because the number of normal modes of vibration decreases from 36 to 24 in going from CaMeCp to CaPy. Modes ν_{12} and ν_{13} are totally symmetric in C_s point group symmetry, while ν_{24} is not. Thus ν_{24} is expected only to be observed as even quanta overtones in the electronic spectra of CaPy.

In section A3, we briefly discussed some aspects of the assignment of the excitation spectrum of CaPy shown in Figure 8, including assignment of the $\tilde{A}$–$\tilde{X}$, $\tilde{B}$–$\tilde{X}$, and $\tilde{C}$–$\tilde{X}$ 0_0^0 bands. Here, we concentrate on assignments of the vibrational structure. We therefore assign the bands at 14572 (+248) and 14623 (+231) cm^{-1} as the 12_0^1 bands for the $\tilde{A}$–$\tilde{X}$ and $\tilde{B}$–$\tilde{X}$ band systems, respectively (Table IV). It should be noted that our measured frequency for ν_{12} of 248 cm^{-1} for the $\tilde{A}$ state is in reasonable agreement with that reported by Bopegedera et al.[9] (241 cm^{-1}). However, the frequency measured for ν_{12} by Bopegedera et al. of 249 cm^{-1} for the $\tilde{B}$ state is significantly different from our value of 231 cm^{-1}. Notice, however, that in Figure 8, we have also observed a band corresponding to a vibrational frequency of 247 cm^{-1} associated with the $\tilde{B}$–$\tilde{X}$ system. Bopegedera et al. were unable to obtain sufficient resolution in their spectrum (fwhm ~ 50 cm^{-1}) to resolve the two bands located at +231 and +247 cm^{-1} from the $\tilde{B}$–$\tilde{X}$ origin. We believe that the 247-cm^{-1} interval is not due to ν_{12} but is actually due to $2\nu_{24}$ ($\tilde{B}$). We have two pieces of evidence supporting this claim. First, the band at 14639 (+247) cm^{-1} is weaker than that at 14623 (+231) cm^{-1}, which makes us favor assigning the 231-cm^{-1} band to the fully-allowed Ca–Py stretch, ν_{12}, and the band at 247 cm^{-1} to the overtone of the asymmetric Ca–Py bend, ν_{24}. Secondly, a similar vibrational feature is observed in the $\tilde{A}$–$\tilde{X}$ system where the medium-intensity 24_0^2 band at 14595 cm^{-1} is just to the blue of the stronger 12_0^1 band at 14572 cm^{-1}. The unusually large intensities of the 24_0^2 bands presumably come from a strong Fermi resonance interaction between ν_{12} and $2\nu_{24}$ in the $\tilde{A}$ and $\tilde{B}$ electronic states, paralleling the case of CaMeCp. For the $\tilde{C}$–$\tilde{X}$ band system, we assign the strongest band at 15029 cm^{-1} to the blue of the $\tilde{C}$–$\tilde{X}$ origin as the 12_0^1 transition. This gives the $\tilde{C}$ state a Ca–Py stretching frequency of 289 cm^{-1}. In line with our assignments for the $\tilde{A}$–$\tilde{X}$ and $\tilde{B}$–$\tilde{X}$ band systems, a band at 15063 (+332) cm^{-1} is assigned to the $\tilde{C}$–$\tilde{X}$ 24_0^2 transition. In the work of Bopegedera et al., the frequency for ν_{12} ($\tilde{C}$) was not reported, presumably because of the high density of vibronic bands in the vicinity of the $\tilde{C}$–$\tilde{X}$ 12_0^1 band. As pointed out above, there is a third skeletal mode of CaPy, the symmetric Ca–Py bend, ν_{13}, which if active should not be restricted by symmetry selection rules. However, in all three band systems, no clear evidence of excitation of ν_{13} has been observed. As we will see shortly, the absence of an observable progression in ν_{13} offers some uncertainties to the presumed ring-bonding scheme adopted by CaPy.

Table VIII. Vibrational Frequencies[a] of CaPy and d_4-CaPy

	CaPy				d_4-CaPy		
mode[b]	$\tilde{X}$	$\tilde{A}$	$\tilde{B}$	$\tilde{C}$	$\tilde{A}$	$\tilde{B}$	$\tilde{C}$
ν_9[c]	–	797	753	–	566	524	–
ν_{11}	–	598	595	–	–	–	–
ν_{12}	316	248	231	289	232	226	290
$2\nu_{24}$	–	271	247	332	253	246	312

[a] In cm^{-1}. [b] ν_9 is the a′ CH wag, ν_{11} is the a′ ring torsion, ν_{12} is the a′ Ca–Py stretch and ν_{24} is the a″ Ca–Py bend. [c] Another possible assignment for this is ν_{10}, another a′ CH wag. See text.

We have also recorded the excitation spectrum of d_4-CaPy, and this is shown in Figure 9. Here, ν_{12} and $2\nu_{24}$ for the $\tilde{A}$ state of CaPy are measured to be 232 and 253 cm^{-1}, respectively, while the corresponding values for the $\tilde{B}$ state are 226 and 246 cm^{-1}, and for the $\tilde{C}$ state the values are 290 and 312 cm^{-1}. For comparison purposes, we have summarized the assigned vibrational frequencies of CaPy in the $\tilde{A}$, $\tilde{B}$, and $\tilde{C}$ electronic states in Table VIII. If CaPy is treated as a pseudodiatomic harmonic oscillator, one would only expect a decrease of ~3 cm^{-1} in the frequencies of the skeletal modes in going from CaPy to d_4-CaPy. Clearly the decrease in the Ca–Py stretching (ν_{12}) and bending ($2\nu_{24}$) frequencies for the $\tilde{A}$ state of CaPy on full deuteration is significantly larger than expected. Presumably, the hydrogen atoms participate to a small degree in the skeletal vibrational motion in the $\tilde{A}$ state. In the $\tilde{B}$ state, the frequency of the overtone $2\nu_{24}$ is unaffected by deuteration whereas ν_{12} decreases in frequency. The opposite is true for the $\tilde{C}$ state, with ν_{12} being unaffected and $2\nu_{24}$ decreasing on deuteration. As in CaPy, no evidence of ν_{13} excitation is observed in d_4-CaPy.

In the dispersed fluorescence spectrum of CaPy shown in Figure 10, only the Ca–Py stretch (ν_{12}) is observed to be excited. Our measured value of 316 cm^{-1} for ν_{12} in the ground state is again in agreement with that of 311 cm^{-1} reported in ref 9. The fact that only the fully-allowed Ca–Py stretch is observed in Figure 10 is quite surprising since, in the excitation spectrum, Fermi resonance interaction between the excited electronic states 12^1 and 24^2 vibrational levels allow the overtone bands of ν_{24} to be observed with medium intensities. Presumably, the absence of any band attributable to 24_2 in Figure 10 is due to a significantly weaker Fermi resonance interaction between ν_{12} and $2\nu_{24}$ levels in the ground state than in the excited states of CaPy.

Table IX. Comparison of the Skeletal Modes of CaCp, CaMeCp, and CaPy

	CaCp			CaMeCp			CaPy			
mode[a]	$\tilde{X}$	$\tilde{A}^2E_{1(1/2)}$	$\tilde{A}^2E_{1(3/2)}$	$\tilde{X}$	$\tilde{A}$	$\tilde{B}$	$\tilde{X}$	$\tilde{A}$	$\tilde{B}$	$\tilde{C}$
M–R stretch	311	329	329	297	307	304	316	248	231	289
M–R bend (s)	–	–	–	143	139	150	–	–	–	–
M–R bend (a)	–	444	431	337	349	350	–	271	247	332

[a] Symmetric = s, asymmetric = a.

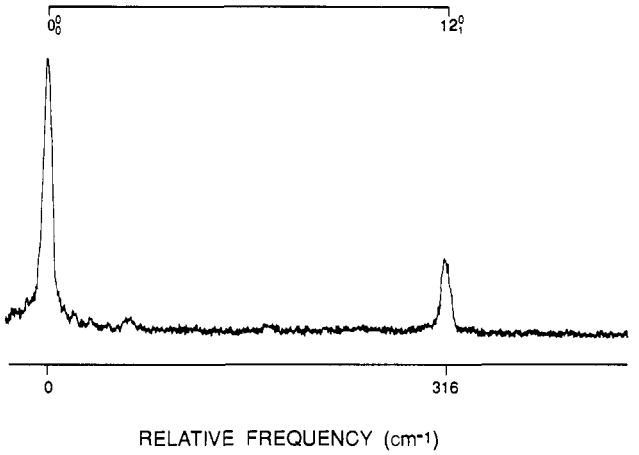

Figure 10. Dispersed fluorescence spectrum of CaPy obtained by pumping the $\tilde{B}$–$\tilde{X}$ 0_0^0 band at 14392 cm^{-1}.

(b) Intra-Ring Vibrations. The structure in the excitation spectrum of CaPy above 14700 cm^{-1} is very complex. In this region, many of the bands presumably arise from ring vibrations. The density of bands relative to the case of CaCp is no surprise given the lower point group symmetry of CaPy (presumed to be C_s but see comments in the next section) compared to that of CaCp (C_{5v}), which gives rise to more totally symmetric ring vibrations in CaPy than there are in CaCp. Furthermore, we also have to consider the fact that there are three overlapping band systems, $\tilde{A}$–$\tilde{X}$, $\tilde{B}$–$\tilde{X}$, and $\tilde{C}$–$\tilde{X}$. Given the large number of vibronic bands of CaPy above 14700 cm^{-1}, serious difficulties are encountered in making vibrational assignments. However, there are a few bands in the proximity of the $\tilde{C}$–$\tilde{X}$ origin band which appear to belong to the $\tilde{A}$–$\tilde{X}$ and $\tilde{B}$–$\tilde{X}$ systems, which we should be able to assign with reasonable confidence. We will confine our analysis of the intra-ring vibrations to this region.

For CaPy, there are 21 intra-ring modes,[17] 11 of which are totally symmetric under C_s point group symmetry. Of the totally symmetric modes, four have frequencies which are generally expected to be <1000 cm^{-1}, which falls within the spectral region we are focusing on. These modes are ν_8 (ring deformation), ν_9 (CH wag), ν_{10} (CH wag), and ν_{11} (ring torsion).[17] The ring torsion mode, ν_{11}, is expected to have the lowest frequency (~600 cm^{-1}) among these modes. We therefore tentatively assign the bands at 14922 (+598) and 14987 (+595) cm^{-1} as being due to the 11_0^1 transitions for the $\tilde{A}$–$\tilde{X}$ and $\tilde{B}$–$\tilde{X}$ systems, respectively. There are two more bands which we can assign with reasonable confidence, those at 15121 (+797) and 15145 (+753) cm^{-1}. In ref 10, ν_9 (CH wag) was found to have a frequency of ~815 cm^{-1}. Therefore, we attribute the bands at 15121 and 15145 cm^{-1} as being the $\tilde{A}$–$\tilde{X}$ and $\tilde{B}$–$\tilde{X}$ 9_0^1 bands, respectively. It is, however, pertinent to point out that ν_{10} (which is also a CH wag) is another possible candidate for such a spacing since in ref 17, ν_{10} was found to have a frequency of ~730 cm^{-1}. Convincing experimental evidence in favor of assigning the 797 and 753-cm^{-1} bands to a CH wag comes from the excitation spectrum of d_4-CaPy. Here, the bands at 15121 and 15145 cm^{-1} observed in the CaPy spectrum are absent, and two new bands at +563 and +532 cm^{-1} relative to the $\tilde{A}$–$\tilde{X}$ and $\tilde{B}$–$\tilde{X}$ origin bands of d_4-CaPy, respectively, are observed, spacings which are entirely consistent with a hydrogenic motion.

A summary of the frequencies of the vibrational modes of CaPy and d_4-CaPy observed in this work is given in Table VIII.

(c) Ring-Bonding or N-Bonding? The ring-bonding scheme adopted by CaCp and CaMeCp is clearly verified by their electronic spectra. However, in the case of CaPy, the equilibrium location of the metal atom is perhaps less obvious. To assist in addressing this issue, a comparison of the skeletal modes of CaCp, CaMeCp, and CaPy is given in Table IX. In CaMeCp, the ring-bonding mode is confirmed by the presence of single quantum excitation of the symmetric M–ring bend (ν_{20}) and the overtone of the asymmetric M–ring bend (ν_{36}). Unfortunately, in CaPy, only the overtone of the M–ring bend (ν_{24}) is observed. This could mean either one of two things: (i) Ca^+ is N-bonded since under C_{2v} symmetry the two M–ring bends are both asymmetric and therefore are expected to be observed only as overtones, or (ii) Ca^+ is ring-bonded (C_s symmetry) but the Ca^+ ion is not significantly displaced from its equilibrium position along the plane of symmetry of the molecule on electronic excitation, and therefore there is no activity in the symmetric M–ring bending mode (ν_{13}). We note that in the case of CdPy and ZnPy,[17] ν_{13} was not active at all on $\tilde{A}$–$\tilde{X}$ excitation but still these molecules were shown to be ring-bonded in their $\tilde{X}$ and $\tilde{A}$ states.

The M–ring stretching frequencies for CaCp, CaMeCp, and CaPy are comparable in magnitude in their ground states. This strongly suggests that in the ground state of CaPy, the metal atom is ring-bonded in approximately the same manner as CaCp and CaMeCp. However, the same conclusion cannot be reached for the excited states of CaPy. In CaPy and CaMeCp, an increase in the M–ring stretching frequency is observed on $\tilde{A}$–$\tilde{X}$ (and $\tilde{B}$–$\tilde{X}$ for CaMeCp) excitation, which implies stronger bonding in their excited states. The opposite is true for CaPy, where we see a significant decrease in the frequency of the M–ring stretch (and therefore of the bond strength) in going from the ground to the excited states. Since we see a quite simple Franck–Condon pattern in Figure 8, i.e., we do not see long progressions in any vibrational mode, it is clear, that a decrease (rather than an increase as in CaCp and CaMeCp) in the Ca–Py stretching frequency does not mean that the bonding scheme in the ground state is completely different from that in the excited states. In other words, the metal does not change from being ring-bonded to being N-bonded on excitation. Instead, we suspect that the decrease in Ca–ring bond strength on excitation is due to the higher degree of ionicity of the M–ring bond in CaPy compared with those in CaCp and CaMeCp. The more ionic nature of the Ca–Py bond would be expected if we base our arguments on the electron affinities of the Py, Cp, and MeCp radicals, which have been measured to be $\simeq$2.39 ± 0.12,[31] 1.786 ± 0.020,[32] ≤1.67 ± 0.04 eV,[33] respectively. The higher electron affinity of the Py radical comes as a result of the fact that N is more electronegative than C. As pointed out by Kershner et al.,[34] this difference in electronegativity between N and C results in a greater tendency for electron withdrawal from the metal atom by the heterocyclic Py ring than by the carbocyclic Cp ring. This electron-withdrawing effect of N in the pyrrolyl ring also reduces the π-complexing ability of Py (and therefore the degree of covalency of the Ca–Py bond), the most important binding property of π-ring systems, which in turn makes pyrrolyl-containing organometallic compounds relatively unstable and fairly hard to synthesize.[34-37] In the $\tilde{X}$ state of CaCp,

(31) Richardson, J. H.; Stephenson, L. M.; Brauman, J. I. *J. Am. Chem. Soc.* **1975**, *97*, 1160.
(32) Engelking, P. C.; Lineberger, W. C. *J. Chem. Phys.* **1977**, *67*, 1412.
(33) Richardson, J. H.; Stephenson, L. M.; Brauman, J. I. *J. Chem. Phys.* **1973**, *59*, 5068.
(34) Kershner, D. L.; Rheingold, A. L.; Basolo, F. *Organometallics* **1987**, *6*, 196.

Table X. Comparison of the $\tilde{A}$–$\tilde{X}$ Transition Frequencies[a] for Various Ca-Containing Radicals

molecule	$\tilde{A}$–$\tilde{X}$ transition freq[b]	molecule	$\tilde{A}$–$\tilde{X}$ transition freq[b]
CaPy[c]	14324	$CaOCH_3$[h]	15917
CaMeCp[c]	14465	CaOH[h]	15965
CaCp[c]	14508	CaBr[g]	15986
$CaCH_3$[d]	14703	CaCl[g]	16094
CaSH[e]	15366	CaNC[i]	16191
$CaNH_2$[f]	15464	CaN_3[j]	16217
$CaSCH_3$[e]	15509	CaNCO[k]	16230
CaI[g]	15586	CaF[g]	16490

[a] In cm^{-1}. [b] For molecules with a doubly degenerate $\tilde{A}^2E$ (or $A^2\Pi$ for diatomics and pseudodiatomics) state, the transition frequency given here is from the $\tilde{X}$ (or X) state to the first spin–orbit component of the $\tilde{A}$ (or A) state. [c] This work. [d] References 10 and 11. [e] Reference 38. [f] Reference 30. [g] Reference 39. [h] References 12 and 13. [i] Reference 40. [j] Reference 41. [k] References 42 and 43.

CaMeCp, and CaPy, the unpaired electron is essentially in an sp hybrid orbital (mainly 4s in character) of Ca^+ which due to its shape does not provide effective overlap with the π-orbitals of the ring. But in their excited states, the unpaired electron is located in an orbital of mixed 3d/4p character. As pointed out earlier, the shape of d-orbitals facilitates overlap with the π-ring system, and therefore covalent contributions to the bonding might be important in the excited states. The stronger bonding in the excited states of CaCp and CaMeCp is presumably due to the increased covalent contributions compared with their $\tilde{X}$ states. However, for CaPy, the greater ionicity of this molecule results in more contracted 3d-orbitals on calcium, and this presumably results in ineffective orbital overlap. This may be the major reason for the weaker metal–ring bonding in the excited states of CaPy.

Another convincing piece of evidence which makes us favor the ring-bonding scheme in CaPy is the frequency of the $\tilde{A}$–$\tilde{X}$ 0_0^0 transition compared to those of other Ca-containing radicals. In Table X, we arrange the known $\tilde{A}$–$\tilde{X}$ 0_0^0 transition frequencies of several Ca-containing radicals in order of increasing magnitude. A trend can be identified from this table, namely, that in general, the $\tilde{A}$–$\tilde{X}$ (or A–X for diatomics) transition moves further to the blue as the electronegativity of the ligand increases. For example, all the calcium monohalides[39] have A–X transition frequencies above 15500 cm^{-1}, while at the other extreme, those of the calcium alkyl radicals are around 14500 cm^{-1}. In Table X, there are also several radicals where the ligand contains a nitrogen atom. For example, $CaNH_2$ (15464 cm^{-1}),[30] CaNC (16191 cm^{-1}),[40] CaN_3 (16217 cm^{-1}),[41] and CaNCO (16230 cm^{-1})[42,43] are all known to be N-bonded, and their $\tilde{A}$–$\tilde{X}$ 0_0^0 transition frequencies (given in parenthesis) are all above 15400 cm^{-1}. On the other hand, that of CaPy is at 14324 cm^{-1}, a transition frequency comparable in magnitude, not to those N-bonded radicals mentioned above, but to those of CaMeCp and CaCp, both of which are ring-bonded. This evidence, coupled with that presented earlier, means that CaPy is almost certainly ring-bonded rather than N-bonded.

C. Internal Rotation of the Methyl Group in CaMeCp. Very low-frequency bands are observed in the $\tilde{A}$–$\tilde{X}$ system of CaMeCp, which cannot be attributed to any of the skeletal or intra-ring vibrational modes described in the previous section. These features are observed to be built upon the $\tilde{A}$–$\tilde{X}$ 0_0^0 and 19_0^1 bands. This is shown clearly in Figure 6, which represents an expanded portion of the spectrum near the $\tilde{A}$–$\tilde{X}$ origin band. Since no similar bands were observed in CaCp and given that these features are also irregularly spaced, we attribute these transitions to excitation of methyl torsional motion.

Table XI. Methyl Torsional Parameters[a] for MeCp-Containing Radicals

molecule	ground state ($\tilde{X}$) V_3	ground state ($\tilde{X}$) V_6	excited state V_3	excited state V_6
$C_5H_4CH_3$[b]	0[c]	48.8	0[c]	211.5
$CH_3C_5H_4$-He_2[b]	0[c]	51.0	0[c]	237.6
$ZnC_5H_4CH_3$[d,e]	170	−85	41	10
$CdC_5H_4CH_3$[d,e]	133	−45	58	−30
$CaC_5H_4CH_3$[d,f]	152	20	101	17

[a] In cm^{-1}. [b] The excited state refers to the $\tilde{B}$ state. See refs 20 and 21. [c] V_3 is zero by symmetry. See refs 20 and 21. [d] The reduced rotational constant, B, was fixed at 5.2 cm^{-1} in the fit. We found that small variations of B have no significant impact on the quality of the fit. [e] The excited state refers to the $\tilde{B}$ state. See ref 18. [f] The excited state refers to the $\tilde{A}$ state. This work.

The potential energy, $V(\phi)$, which hinders rotation of the methyl group in CaMeCp, is a periodic function of ϕ, the angle of internal rotation, and can be expressed in a general form as a Fourier series expansion:

$$V(\phi) = \tfrac{1}{2} \sum_n V_n(1 - \cos n\phi) \qquad (1)$$

where n in effect represents the number of potential minima or maxima generated in a 2π revolution. In the case of CaMeCp, symmetry restricts the allowed values of n to 3, 6, 9, ... Due to the normally rapidly decreasing magnitudes of V_n as n increases, we will retain only the first two terms in the expansion, V_3 and V_6. As is usual, we will assume to a first approximation that the internal rotation of the methyl group can be fully separated from the other vibrational modes of the molecule, i.e., there is negligible interaction (or mixing) of the methyl torsion with the other low-frequency vibrations of the molecule.

One can model internal rotation of the methyl group in CaMeCp by substituting eq 1 into a simple one-dimensional Schrödinger equation of the form:[44]

$$B \frac{d^2\Psi(\phi)}{d\phi^2} + [E - V(\phi)]\Psi(\phi) = 0 \qquad (2)$$

Here, B is the reduced rotational constant for the methyl rotation.

We have given a description of the method used to calculate the energies of the methyl torsional levels of a molecule such as CaMeCp elsewhere.[18] Briefly, the torsional Hamiltonian matrix is diagonalized in a one-dimensional free rigid rotor basis. The potential function parameters, V_3 and V_6, in the $\tilde{A}$ electronic state of CaMeCp are determined by adjusting their values until the calculated torsional frequencies give a best fit to the observed torsional frequencies. The value for the reduced rotational constant B is fixed at a reasonable value of 5.2 cm^{-1} since small variations in B were found to have no significant impact on the quality of the fit.

In describing the symmetry of nonrigid molecules, one must use the molecular symmetry group.[45,46] For CaMeCp, the appropriate molecular symmetry group is G_6 which is isomorphous to the C_{3v} point group. Thus, the torsional levels of CaMeCp are denoted by the symmetry species a_1, a_2, and e of the C_{3v} point group and also by the torsional quantum number m. The selection rules for the methyl torsional transitions are $a_1 \leftrightarrow a_1$, $a_2 \leftrightarrow a_2$, and $e \leftrightarrow e$. The $a_1 \leftrightarrow a_2$ transition is only allowed if there is a

(35) Ji, L.; Kershner, D. L.; Rerek, M. E.; Basolo, F. *J. Organomet. Chem.* **1985**, *296*, 83.
(36) King, R. B.; Bisnette, M. B. *Inorg. Chem.* **1964**, *3*, 796.
(37) Efraty, A.; Jubran, N. *Inorg. Chim. Acta* **1980**, *44*, L191.
(38) Fernando, W. T. M. L.; Ram, R. S.; O'Brien, L. C.; Bernath, P. F. *J. Phys. Chem.* **1991**, *95*, 2665.
(39) Huber, K. P.; Herzberg, G. *Molecular Spectra and Molecular Structure. IV. Constants of Diatomic Molecules*; Van Nostrand Reinhold: New York, 1979.
(40) Douay, M.; Bernath, P. F. *Chem. Phys. Lett.* **1990**, *174*, 230.
(41) Brazier, C. R.; Bernath, P. F. *J. Chem. Phys.* **1988**, *88*, 2112.
(42) Ellingboe, L. C.; Bopegedera, A. M. R. P.; Brazier, C. R.; Bernath, P. F. *Chem. Phys. Lett.* **1986**, *126*, 285.
(43) O'Brien, L. C.; Bernath, P. F. *J. Chem. Phys.* **1988**, *88*, 2117.
(44) Owen, N. L. Studies of Internal Rotation by Microwave Spectroscopy. In *Internal Rotation in Molecules*; Orville-Thomas, W. J., Ed.; John Wiley and Sons: London, 1974, pp 157–215.
(45) Longuet-Higgins, H. C. *Mol. Phys.* **1963**, *6*, 445.
(46) Bunker, P. *Molecular Symmetry and Spectroscopy*; Academic Press: London, 1979.
(47) Spangler, L. H.; Pratt, D. W. *J. Chem. Phys.* **1986**, *84*, 4789.

Table XII. Torsional Transition Frequencies[a] of CaMeCp

$\tilde{A}$–$\tilde{X}$	Obsd[b]	Calcd[b,c]
Excitation Spectrum		
4e–1e	108	109.4
$3a_1$–$0a_1$	82	81.8
$3a_2$–$0a_1$	67	68.2
2e–1e	55	54.9
1e–1e	0	0.5
$0a_1$–$0a_1$	0	0.0
Dispersed Fluorescence Spectrum		
1e–2e	75	74.5
$0a_1$–$3a_2$	81	81.6
$0a_1$–$3a_1$	118	112.2
1e–4e	131	133.5

[a] In cm^{-1}. [b] Frequency relative to origin band. [c] Calculated from the constants in Table XI.

strong coupling between internal rotation of the methyl group and overall rotation of the molecule. As we will see shortly, we do indeed observe this transition.

As summarized in Table XI, the 3-fold barrier to methyl free rotation (V_3) in the $\tilde{A}$ state of CaMeCp is determined to be 101 cm^{-1}. A positive value of 17 cm^{-1} for V_6 is obtained, which essentially makes the bottom of the potential well narrower and that of the maximum broader without changing the height of the 3-fold barrier. A comparison of the calculated torsional transition frequencies and those which are observed in Figure 6 is given in Table XII. There is clearly excellent agreement between the two sets of data. We are then able to assign with reasonable confidence the torsional transitions in the $\tilde{A}$–$\tilde{X}$ system of CaMeCp, and these assignments are specified in Table XII.

To determine the corresponding values for V_3 and V_6 in the ground state of CaMeCp and to verify our initial assignment of the torsional bands in the excitation spectrum, we have recorded dispersed fluorescence spectra of CaMeCp by pumping each of the torsional bands. These spectra are shown in Figure 11. Obtaining a reasonable signal-to-noise ratio in the dispersed fluorescence spectra of CaMeCp proved to be difficult for two reasons: (i) the torsional bands in the excitation spectrum are quite weak, and (ii) the sensitivity of our diode array detector is quite low at the relatively long emission wavelengths (~690 nm) of CaMeCp. To compensate for these limitations and still maximize the signal, the detection gate was not delayed sufficiently to remove all of the scattered dye laser light. Thus the intensity of the band at the pump position is not representative of the actual emission from CaMeCp at the frequency of the dye laser. Unfortunately, the actual contribution of the scattered laser light cannot be inferred accurately from these traces.

Figure 7a shows the dispersed fluorescence spectrum obtained by pumping the $\tilde{A}$–$\tilde{X}$ 0_0^0 band. The pump laser frequency accesses both the $0a_1$–$0a_1$ and 1e–1e methyl torsional transitions, since as shown in Table XII, the calculated energy separation between these two transitions is only ~0.5 cm^{-1}. This is further confirmed by the emission emanating from these two excited state torsional levels, where we see emission to both e and a (a_1 and a_2) levels in the ground state. We have also recorded the dispersed fluorescence spectra following excitation of each of the other torsional transitions indicated in Figure 6. As expected, the a_1–a_1, a_2–a_2 (and a_1–a_2), and e–e symmetry selection rules are obeyed giving rise to the expected differences in the spectra when the e and a (a_1 and a_2) levels were pumped. Thus these spectra confirm our assignments for the torsional structure in the excitation spectrum. Furthermore, the presence of skeletal vibrational structure arising from ν_{19} and $2\nu_{36}$ built upon these torsional levels in the $\tilde{X}$ state proves beyond any doubt that these bands do indeed originate from CaMeCp. From the observed torsional levels of CaMeCp in the ground state, the methyl torsional potential parameters are determined to be V_3 = 152 cm^{-1} and V_6 = 20 cm^{-1}. Again, the B constant has been fixed at a value of 5.2 cm^{-1}.

A summary of the barrier heights in both $\tilde{X}$ and $\tilde{A}$ electronic states of CaMeCp is presented in Table XI. For comparison purposes, we have also included the corresponding values for other

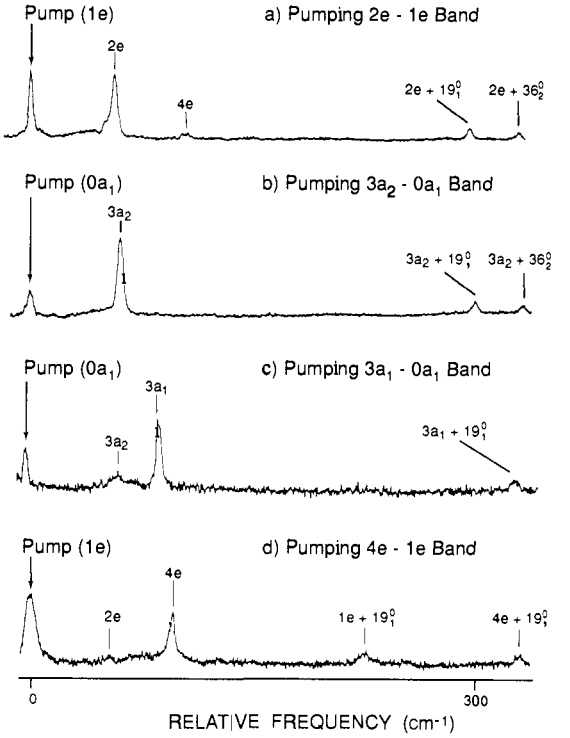

Figure 11. Dispersed fluorescence spectra of CaMeCp obtained by pumping methyl torsional bands. (a) Pumping the $\tilde{A}$–$\tilde{X}$ 2e–1e band at 14 520 cm^{-1}. (b) Pumping the $\tilde{A}$–$\tilde{X}$ $3a_2$–$0a_1$ band at 14 532 cm^{-1}. (c) Pumping the $\tilde{A}$–$\tilde{X}$ $3a_1$–$0a_1$ band at 14 547 cm^{-1}. (d) Pumping the $\tilde{A}$–$\tilde{X}$ 4e–1e band at 14 573 cm^{-1}. All the spectra shown in this figure were recorded with some laser scattered light contributing at the pump position. See text for details.

related molecules, namely, bare MeCp, the inert gas–radical complex MeCp–He_2, and the organometallic radicals ZnMeCp and CdMeCp.

In ref 20, the relatively high 6-fold barrier (V_6) in the bare MeCp radical is attributed to a hyperconjugative effect, where the methyl group (acting as an electron "donor"), if aligned in an effective geometric fashion with the π-orbitals of the electron-deficient ring, is "locked" in this position. However, in the case of CaMeCp, hyperconjugation between the methyl group and the C_5H_4 ring is essentially absent because in both its $\tilde{X}$ and $\tilde{A}$ electronic states, the $MeCp^-$ ring has an aromatic sextet of electrons. Furthermore, the metal atom is bonded to one side of the ring creating a completely different electron density distribution above and below the ring. It is this effect that gives rise to the relatively high 3-fold barriers, as shown in Table XI, which dominate over the V_6 terms. Further examination of Table XI reveals that in the ground electronic state of CaMeCp, the 3-fold barrier (V_3) for CaMeCp is quite similar in magnitude to those of the ground states of ZnMeCp and CdMeCp. Quite possibly, this may be attributed to the fact that for the $\tilde{X}$ states of these three MMeCp molecules, the unpaired electron resides in an MO which is thought to be mainly metal ns in character (n = 4 for Ca and Zn and 5 for Cd). As in ZnMeCp and CdMeCp, we believe that the metal atom in CaMeCp is located far enough from the methyl group so as to avoid any direct steric hindrance to free rotation of the methyl group. Consequently, as stated above, we believe that the large V_3 term is a result of an electronic rather than a steric effect. Furthermore, notice that V_3 for CaMeCp in its $\tilde{A}$ electronic state is about a factor of 2 larger than those of the $\tilde{B}$ states of ZnMeCp and CdMeCp. This difference presumably also arises mainly from an electronic effect. As discussed in ref 18 and in section IIIA2, the electronic structure in the $\tilde{A}$ state of CaMeCp is thought to be very different from those of the $\tilde{B}$ states of ZnMeCp and CdMeCp. In CaMeCp, the unpaired electron is located in an MO which is essentially a Ca^+ 3d–4p mixed orbital. In contrast, in the $\tilde{B}$ states of ZnMeCp and CdMeCp, the unpaired electron is in an MO which is mainly C

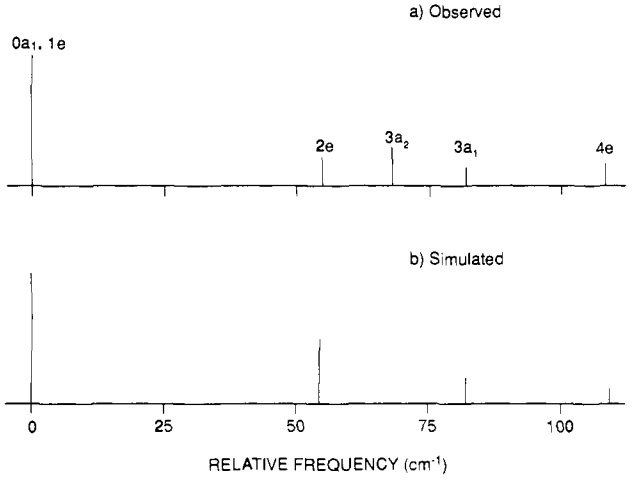

Figure 12. Stick diagram of the (a) observed and (b) simulated excitation spectra of CdMeCp near the $\tilde{A}$–$\tilde{X}$ origin band. Diagram a represents the average of three scans around the $\tilde{A}$–$\tilde{X}$ origin. See text for discussion.

$2p\pi$ in character (see the discussion on the electronic structure of ZnCp and CdCp in ref 15 for more details).

Generally, if there is no shift in the phase angle, θ, between the minima of the ground and excited electronic state torsional potential wells, i.e., there is no change in methyl group conformation, only the $0a_1$–$0a_1$ and 1e–1e transitions will be observed with any significant intensity from Franck–Condon arguments. Presumably, this is the reason why in the $\tilde{B}$–$\tilde{X}$ band system of CaMeCp, transitions to the higher torsional levels are not seen in Figure 5. However, this is not the case for the $\tilde{A}$–$\tilde{X}$ system of CaMeCp, as discussed above. The 2e–1e, $3a_2$–$0a_1$, $3a_1$–$0a_1$, and 4e–1e transitions are all observed, which implies immediately that θ is significantly different from 0 for the $\tilde{A}$–$\tilde{X}$ transition. The actual value for θ can be determined from the relative intensities of the torsional bands. As described by Spangler and Pratt,[47] the Franck–Condon factors (FCFs) for the various torsional transitions can be achieved using the eigenvectors obtained by matrix diagonalization of the torsional Hamiltonian. We have performed such calculations for the appropriate torsional transitions of CaMeCp. The closest agreement between the calculated and experimental intensities of the torsional bands for both the excitation and dispersed fluorescence spectra is obtained when a value of 30° for θ is used. To illustrate this, we show in Figure 12 the calculated and observed excitation spectrum of CaMeCp in stick diagram fashion. The agreement in intensities is clearly quite good with the possible exception of the 2e–1e transition. In the case of the a_1–a_2 transition, its intensity cannot be simulated simply by the Franck–Condon factor (which is 0) since this transition becomes allowed only if overall rotation of the molecule is taken into account.

IV. Conclusion

Laser excitation and dispersed fluorescence spectra of CaCp, CaMeCp, and CaPy have been presented and discussed. These spectra showed extensive vibrational structure which was attributed to excitation of both skeletal and intra-ring modes. From this structure, we were able to confirm that a ring-bonding scheme is adopted by these molecules in the gas phase, as suggested earlier by Bernath and co-workers.[8,9] The electronic spectra of d_5-CaCp and d_4-CaPy were employed to assist in the assignment of intra-ring vibrations of CaCp and CaPy. Strong evidence of single quantum excitation of two of the six e_2 modes of CaCp was observed which indicates that this molecule is Jahn–Teller active in its $\tilde{A}^2E_1$ electronic state.

In the case of CaMeCp, very low-frequency, irregularly spaced bands were attributed to hindered rotation of the methyl group. From this structure, the barriers to methyl free rotation in the $\tilde{X}$ and $\tilde{A}$ electronic states of CaMeCp were determined as well as the change in conformation of the methyl group on $\tilde{A}$–$\tilde{X}$ excitation.

Acknowledgment. We would like to thank the National Science Foundation for support of this work via Grant No. CHE-9005963. A.M.E. gratefully acknowledges the award of a NATO/SERC and Ohio State postdoctoral fellowships during his stay at The Ohio State University. E.S.J.R. greatly appreciates the award of a 1991 Rohm and Haas and a 1992 Phillips Petroleum fellowships.

Photochemistry of Matrix-Isolated Diazoethane and Methyldiazirine: Ethylidene Trapping?

Randal A. Seburg[1] and Robert J. McMahon*

Contribution from the Department of Chemistry, University of Wisconsin, Madison, Wisconsin 53706. *Received March 24, 1992*

Abstract: Photolysis of matrix-isolated diazoethane (**1a**) at 8 K produces mainly ethene (**4a**), along with a small amount of 3-methyldiazirine (**2a**). ESR experiments employing a variety of irradiation conditions and matrix media (Ar, N_2, Xe) show that triplet ethylidene (**3T**) is not an observable photoproduct. Similar experiments fail to reveal direct evidence for either singlet or triplet ethylidene by IR or UV–vis spectroscopy. Photolysis of nascent 3-methyldiazirine (**2a**) also fails to yield ethylidene. Deuterium substitution produces no detectable change in the chemistry. In carbon monoxide-doped matrices, photolysis of **1** generates 3-methyldiazirine (**2**) and ethene (**4**) as well as a small amount of methylketene (**5**). The most plausible interpretation of these results postulates that (i) trapping of incipient singlet ethylidene (**3S**) by CO competes with the facile hydrogen migration and (ii) intersystem crossing to the triplet does not compete with hydrogen migration.

Carbenes frequently rearrange via intramolecular 1,2-hydrogen migrations to form alkenes. Both theoreticians and experimentalists have expended considerable effort investigating these facile rearrangements.[2,3] Ethylidene (**3**, methylcarbene) holds special

0002-7863/92/1514-7183$03.00/0